



**UNIVERSIDAD DE INVESTIGACIÓN DE TECNOLOGÍA
EXPERIMENTAL YACHAY**

Escuela de Ciencias Físicas y Nanotecnología

**TÍTULO: CHARACTERIZATION OF INDIVIDUALIZED
HiPco® SINGLE WALLED CARBON NANOTUBES IN DRIED
DMF USING POTASSIUM AND SODIUM AS CHARGE
TRANSFER DONORS**

Trabajo de integración curricular presentado como requisito para la
obtención del título de Ingeniera en Nanotecnología

Autor:

Layana Franco Lorena A.

Tutor:

Dr. rer. nat. Chacón Torres Julio C.

Urququí, agosto de 2019

Urcuquí, 20 de agosto de 2019

SECRETARÍA GENERAL
(Vicerrectorado Académico/Cancillería)
ESCUELA DE CIENCIAS FÍSICAS Y NANOTECNOLOGÍA
CARRERA DE NANOTECNOLOGÍA
ACTA CONSOLIDADA DE FINALIZACIÓN DE ESTUDIOS No. UITEY-PHY-2019-00005-AC

En la ciudad de San Miguel de Urcuquí, Provincia de Imbabura, a los 20 días del mes de agosto de 2019, se emite la presente acta consolidada de finalización de estudios, conforme lo establecido en el artículo 101 del Reglamento de Régimen Académico aprobado por el Consejo de Educación Superior (CES), mediante resolución RPC-SO-08-No.111-2019, de 27 de febrero de 2019.

DATOS DE IDENTIFICACIÓN DEL ESTUDIANTE

Documento de Identificación	Apellidos y Nombres	Carrera
0921682761	LAYANA FRANCO, LORENA ALEXANDRA	NANOTECNOLOGÍA

SUFICIENCIA DE LA LENGUA EXTRANJERA

Conforme lo establecido en el artículo 31 del Reglamento de Régimen Académico aprobado por el Consejo de Educación Superior (CES), mediante resolución RPC-SE-13-No.051-2013, de 22 de marzo de 2017: (...) las IES garantizarán el nivel de suficiencia del idioma para cumplir con el requisito de graduación de las carreras de nivel técnico superior, tecnológico superior y sus equivalentes; y, tercer nivel, de grado, deberán organizar u homologar las asignaturas correspondientes desde el inicio de la carrera. La suficiencia de la lengua extranjera deberá ser evaluada antes de que el estudiante se matricule en el último periodo académico ordinario de la respectiva carrera; tal prueba será habilitante para la continuación de sus estudios, sin perjuicio de que este requisito pueda ser cumplido con anterioridad. (...) En las carreras de tercer nivel, de grado, se entenderá por suficiencia en el manejo de una lengua extranjera al menos el nivel correspondiente a B2 del Marco Común Europeo de referencia para las Lenguas. (...)

Calificación	Nivel Alcanzado
84	B2



Mgs. MONTAÑO ORMAZA, DENNYS EDUARDO
Director del Departamento de Inglés

PRÁCTICAS PRE-PROFESIONALES O PASANTÍAS

Conforme lo establecido en los artículos 82, 89, 94 del Reglamento de Régimen Académico aprobado por el Consejo de Educación Superior (CES), mediante resolución RPC-SE-13-No.051-2013, de 22 de marzo de 2017.

Vinculación

Empresa	Nombre Proyecto	Horas	Fecha Inicio	Fecha Fin
UNIDAD EDUCATIVA VICTOR MANUEL GUZMAN	INSPIRATHON	160	08/10/2018	08/12/2018
Total Horas Cumplidas:		160		

Prácticas

Empresa	Horas	Fecha Inicio	Fecha Fin
FRIEDRICH ALEXANDER UNIVERSITAT ERLANGEN NUREMBERG - LAYANA	304	04/06/2018	27/07/2018
Total Horas Cumplidas:		304	



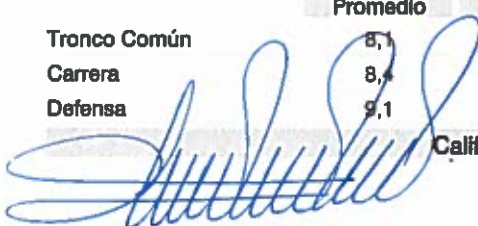
Dra. SALUM, GRACIELA MARISA, Ph.D.
Presidenta de la Comisión de Prácticas Pre-Profesionales y Vinculación con la Sociedad

REGISTRO DE CALIFICACIONES

Conforme lo establecido en el artículo 24 del Reglamento de Titulación de Grado de la Universidad de Investigación de Tecnología Experimental Yachay, en el que establece: La calificación final de grado del estudiante se obtendrá calculando de la siguiente manera: 1. El 70% corresponderá al promedio ponderado de calificaciones obtenidas por el estudiante a lo largo de toda su carrera y que se calculará en relación con el número de horas totales asignadas a cada asignatura en la correspondiente malla curricular distribuido así: a) El 20% para las asignaturas del "Tronco Común"; y, b) El 50% para las asignaturas propias de cada Carrera incluyendo los itinerarios. 2. El 30% restante corresponderá a la calificación de la defensa del trabajo de titulación o del examen teórico – práctico.

Fecha de Inicio: 28/10/2014 Fecha de Finalización: 20/08/2019

	Promedio	Horas	Créditos	Porcentaje	Calificación
Tronco Común	5,1			20 %	1,6
Carrera	8,4	8368	215	50 %	4,2
Defensa	9,1			30 %	2,7
Calificación Final de Grado:				100 %	8,6


Mgs. CASANOVA YANDUN, EDISON GUILLERMO
Director de Registros Académicos

TITULACIÓN

Una vez se ha verificado el cumplimiento de los requisitos establecidos en el artículo 31 del Reglamento de Titulación de Grado de la Universidad de Investigación de Tecnología Experimental Yachay, aprobado mediante Resolución No.RCG-SE-10 No.036-2018 de 28 de septiembre de 2018, se confiere el título de INGENIERO/A EN NANOTECNOLOGÍA, a el(la) señor(ita) LAYANA FRANCO, LORENA ALEXANDRA.

Desde la fecha de suscripción de la presente acta, conforme lo establecido en el artículo 101 del Reglamento de Régimen Académico aprobado por el Consejo de Educación Superior (CES), mediante resolución RPC-SO-08-No.111-2019, de 27 de febrero de 2019; la Universidad de Investigación de Tecnología Experimental Yachay, tiene un plazo de cuarenta y cinco (45) días para registrar el título en el Sistema Nacional de Información de la Educación Superior (SNIESE), previa entrega al graduado.

Para constancia de lo actuado, firman el Secretario General, el Decano de la Escuela y el/la Estudiante.


Dr. BRITO GONZALVEZ, JOAQUIN LUIS, Ph.D.
Secretario General


Dr. MEDINA DAGGER, ERNESTO ANTONIO, Ph.D.
Decano


LAYANA FRANCO, LORENA ALEXANDRA
Estudiante

Autoría

Yo, LORENA ALEXANDRA LAYANA FRANCO, con cédula de identidad 0921682761, declaro que las ideas, juicios, valoraciones, interpretaciones, consultas bibliográficas, definiciones y conceptualizaciones expuestas en el presente trabajo; así como, los procedimientos y herramientas utilizadas en la investigación, son de absoluta responsabilidad de la autora del trabajo de integración curricular. Así mismo, me acojo a los reglamentos internos de la Universidad de Investigación de Tecnología Experimental Yachay.

Urcuquí, agosto de 2019.



Lorena Alexandra Layana Franco

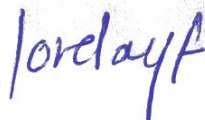
CI: 0921682761

Autorización de Publicación

Yo, LORENA ALEXANDRA LAYANA FRANCO, con cédula de identidad 0921682761, cedo a la Universidad de Tecnología Experimental Yachay, los derechos de publicación de la presente obra, sin que deba haber un reconocimiento económico por este concepto. Declaro además que el texto del presente trabajo de titulación no podrá ser cedido a ninguna empresa editorial para su publicación u otros fines, sin contar previamente con la autorización escrita de la Universidad.

Asimismo, autorizo a la Universidad que realice la digitalización y publicación de este trabajo de integración curricular en el repositorio virtual, de conformidad a lo dispuesto en el Art. 144 de la Ley Orgánica de Educación Superior.

Urcuquí, agosto de 2019.



Lorena Alexandra Layana Franco

CI: 0921682761

Resumen

Los nanotubos de carbono de pared simple (SWCNTs, por sus siglas en inglés) son de gran interés para aplicaciones en futuros productos electrónicos basados en nanomateriales. Las propiedades intrínsecas de los SWCNTs los convierten en candidatos potenciales para aplicaciones particulares como transistores, dispositivos de detección, dispositivos cuánticos de alta densidad, entre otros productos electrónicos innovadores y tecnológicos.

Actualmente, existen varias formas de separar los SWCNTs. Las técnicas habituales para la caracterización de SWCNTs incluyen la espectroscopía Raman, la microscopía de fuerza atómica y la microscopía electrónica de barrido. La combinación de estas técnicas permite identificar el tipo de SWCNT (dando una idea de sus propiedades físicas y electrónicas) y si se mantienen como fueron sintetizados o efectivamente fueron dispersados e individualizados.

En este proyecto de investigación, se obtendrán SWCNTs individualizados a partir de un proceso de exfoliación química que incluye su intercalación con sodio y potasio dispersos en un disolvente seco (dimetilformamida). Aunque el tema principal de este proyecto de investigación fue un nuevo método para desenredar, exfoliar e individualizar SWCNTs, se obtuvo un resultado diferente e interesante: la formación de mallas. Este trabajo podría contribuir al análisis de nanomateriales, caracterización y síntesis de la dispersión de SWCNTs.

Palabras clave: exfoliación, nanomateriales, RBMs, dispersión, GIC

Abstract

Single walled carbon nanotubes (SWCNTs) are of tremendous interest for applications in future nanomaterials-based electronics. The intrinsic properties of SWCNTs make them potential candidates for particular applications such as transistors, sensing devices, high density quantum devices, among other innovative and technological outstanding electronics. Currently, there exist several ways to separate SWCNTs. The usual techniques for SWCNT characterization are Raman spectroscopy, atomic force microscopy and scanning electron microscopy. The combination of these techniques allows to identify the type of SWCNT (giving a insight to their physical and electronic properties) and if they had remained as-synthesized or effectively well dispersed and individualized. In this research project, individualized SWCNTs will be obtained from a chemical exfoliation process that includes their intercalation with sodium and potassium dispersed in a dried optimal solvent (dimethylformamide). Although the main subject of this research project was a new method for the disentanglement, exfoliation and individualization of the SWCNT, a different and interesting result was obtained: the formation of meshes. This work might contribute to nanomaterials analysis-characterization and synthesis of enriched SWCNTs dispersion.

Keywords: exfoliation, nanomaterials, RBMs, dispersion, GIC

Acknowledgements

I will like to express my gratings to Andreas Hirsch and Frank Hauke who put their good faith in accepting a young lady like me at the laboratory of the Joint Institute of Advanced Materials and Processes (Zentralinstitut für neue Materialien und Prozesstechnik, ZMP) of the University Erlangen-Nuremberg in Germany where the experiments of this research thesis were carried out. Thank you also for making possible the accommodations during a stay of two months. Thanks a lot to Claudia Kröckel who was very patient in explaining and guiding me through the synthesis and characterization process. You were also a very supportive friend. Of course, none of this could have been possible without my project supervisor. From the moment I started to work with Julio in 2017 (with other projects), he started to give me encouragement to keep with the hard work. Thank you for trusting in my job and for teaching me as much as you could. You were the main responsible for the research stay in Germany. Thank you for not giving up on that and for not giving up on me. I also appreciate a lot your comments and corrections on the writing of this project. A special thanks to the Chancellor's office of Yachay Tech for buying the airplane tickets and to the School of Physical Sciences of Nanotechnology for trusting in the international research stay. Thanks to all the professors I had in Yachay Tech. Most of them transmit their passion for science and learning to me. Thanks to my family, including my aunts, uncles and cousins because I received all types of support you could possibly give me. Thank you for being my strength during the whole career. Thanks for you understanding, Valeria; even though we were far away from each other, we never stop being best friends. Thanks to Joaquín, your laughs and excitement always took the best of me. I carry the responsibility of being a good example for you and for that I am thankful. I also would like to thank my friends in Guayaquil, they believed in me since day one. I do have a village when I come back to my hometown. Thanks to all of my friends at Yachay Tech who had become my family. You were the immediately people to listen to my stories, tears, laughs, and gave me their best. María José, Gustavo, Andrés, María Rosa, Paul, Bruno, Pepa, Bernardo, Alex, Sebastián and José. Also, big thanks to Charlotte. The research stay in Germany would have not be the same without you. All the moments we have shared (the good and the bad) will stay with me forever. Thank you God, for showing me your infinite love in the bad and good moments.

Contents

List of Figures	ix
List of Tables	xiii
List of Papers	xiv
1 Introduction	1
1.1 The carbon based material: SWCNTs	2
1.2 Properties of SWCNTs	5
1.2.1 Mechanical properties	5
1.2.2 Optical and electronic properties	6
1.3 Synthesis of SWCNTs	9
1.4 Bundles in SWCNTs and their dispersion	10
1.5 Graphite Intercalation Compounds	12
2 Motivation	13
3 Methodology	15
3.1 Synthesis	15
3.1.1 Intercalation compounds	15
3.1.2 Dispersion in the solvent	16
3.2 Scanning Electron Microscopy	16
3.3 Atomic Force Microscopy	18
3.4 Raman Spectroscopy	19

3.4.1	The Raman spectrometer	22
3.4.2	Origin of the characteristic Raman modes for SWCNTs	23
4	Results & Discussion	27
5	Conclusions & Outlook	39
	Bibliography	41

List of Figures

1.1	Orbitals of a Carbon atom.	2
1.2	Representation of a SWCNT (7,2) constructed with its chiral vector and angle. . .	3
1.3	SWCNTs representations for a) zigzag nanotube (5,0), b) armchair nanotube (5,5), chiral nanotube (7,2).	4
1.4	Zone folding axis method applied to graphene to obtain the DOS of SWCNTs. . .	7
1.5	Representation of the DOS of a a) semiconducting and b) metallic SWCNT. . . .	8
1.6	CO flow-tube reactor for high pressure carbon monoxide method.	9
1.7	Lewis structure of DMF.	11
1.8	Schematic illustration of GIC a) stage I and b) stage II.	12
1.9	Exfoliation process starting from GIC.	12
3.1	Diagram for the intercalation compounds synthesis	16
3.2	SEM scheme showing the main elements.	17
3.3	AFM scheme showing the main parts.	19
3.4	Scheme for the scattering of light including Rayleigh, Stokes and Anti-Stokes scattering.	20
3.5	Momentum conservation in an inelastic scattering process according to Equations 3.4 and 3.5.	21
3.6	Scheme of a simplified Raman spectrometer.	22
3.7	Scheme for the Raman scattering processes that give rise to the a) G b) 2D and c) D mode of graphene.	23
3.8	Typical Raman spectrum of SWCNTs presenting the RBM peaks, G^- , G^+ and G' lines.	24

4.1	SEM image of the HiPco [®] SWCNTs in powder.	28
4.2	AFM image of the HiPco [®] SWCNTs dispersed in DMF.	28
4.3	Raman spectrum of the pristine HiPco [®] SWCNTs.	29
4.4	Diagram flow describing the three experiments that were carried out.	31
4.5	Model for the K atoms position in a SWCNTs bundle proposed by Duclaux et al. ⁵⁸	32
4.6	Image of the intercalation compounds and pristine dispersed in DMF	33
4.7	Raman spectra taken with a 532 nm excitation laser, showing the G ⁻ , G ⁺ and G' lines of the GICs from Experiment 1.	34
4.8	GICs from Experiment 1. a) Raman spectra taken with a 532 nm excitation laser of the RBM region b) SEM image of KC ₂₄ , c) SEM image of NaC ₈	34
4.9	GICs from Experiment 2. a) Raman spectra taken with a 532 nm excitation laser of the RBM region, b) SEM image of KC ₂₄ , c) SEM image of NaC ₈	35
4.10	Raman spectra taken with a 532 nm excitation laser of the RBM region of GICs from Experiment 3.	37

List of Tables

1.1	Nanotube type according to n and m	4
4.1	Experimental RBM frequency and reference RBM frequency (ω) and the corresponding assignment of diameter and (n,m) indices for pristine SWCNTs	30
4.2	Experimental RBM frequency and reference RBM frequency (ω) with the corresponding assignment of diameter and (n,m) indices from Experiment 1.	35
4.3	Experimental RBM frequency and reference RBM frequency (ω) with the corresponding assignment of diameter and (n,m) indices from Experiment 2.	36
4.4	RBM experimental and reference RBM frequency (ω) and the corresponding assignment of diameter and (n,m) indexes for Experiment 3.	37

List of Papers

- [1] Luisa Berrezueta, Lorena Layana. Facile route towards the individualization of Single Walled Carbon Nanotubes bundles. JACS Communications. 2019. In preparation.

Chapter 1

Introduction

Alice had no idea what Latitude was, or Longitude either, but thought they were nice grand words to say.

Lewis Carroll

A lot of research has been done around carbon based-material. What is so interesting about carbon materials?, and specially, about single walled carbon nanotubes? For the purpose of some application, will it matter to have the nanotubes as bundles (as synthesized) or as individualize nanotubes? What are the features that can be found when the characterization takes place? The following research thesis project aims to describe and characterize single wall carbon nanotubes that pretend to be individualized via a chemical exfoliation technique. This exfoliation procedure involves the synthesis of intercalation compounds with alkali metals, and their very good dispersion in an organic solvent. There will be some features in the results from the characterization techniques implemented to conclude if the bundles of SWCNTs were individualized.

The questions from the first paragraph will be answered through this work, general concepts and the background of the topics-related will be introduced in this first chapter, and the issues behind the exfoliation of SWCNTs and current methods to resolve it. In the second chapter, the motivation will state the purpose that encourages this research and why it is an important topic. The third chapter will describe the methodology implemented, the fundamentals of the techniques used for the synthesis and characterization. The next chapter will present the results obtained and the corresponding discussion of whether or not the nanotube individualization was

achieved. Finally, the conclusions will summarize and arrive to the final statements about this research project.

1.1 The carbon based material: SWCNTs

A carbon atom has four valence electrons in the $2s$, $2p_x$, $2p_y$ and $2p_z$ orbitals as shown in Figure 1.1 therefore the possibility of forming four bonds with another appropriate atom. According to the molecular orbital theory, a carbon atom forms three sp^2 hybridized orbitals when binding with another carbon atom, three of those bonds are σ bonds, leaving the $2p_z$ orbital perpendicular to the others and forming a π bond¹.

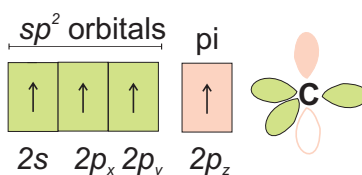


Figure 1.1: Orbitals of a Carbon atom. The sp^2 hybridization and π orbital.

Allotropes are different structural modifications of a chemical element² in the same physical state. Carbon allotropes are structures of a mixture of sp^2 and sp^3 carbon atoms of hexagonal nature³. Among the carbon allotropes are graphite, diamond, fullerenes and amorphous carbon yield carbon nanotubes among others.

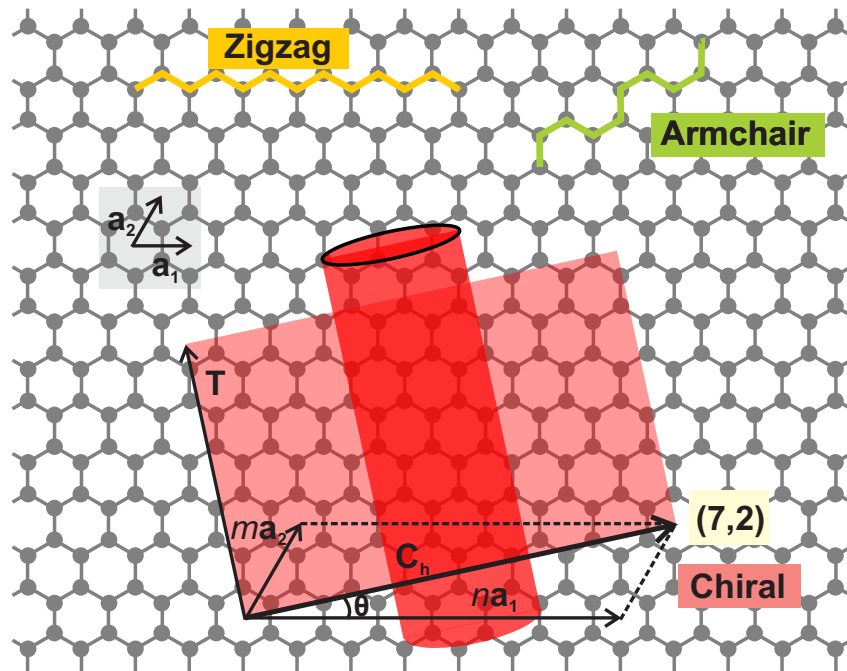


Figure 1.2: Representation of a SWCNT (7,2) constructed with its chiral vector and angle. The SWCNT was generated using the Wolfram Demonstration Projects "Carbon Nanotubes"⁴.

Carbon nanotubes are a 1D nanomaterial that can be thought of as a graphene layer rolled up⁵ as represented in Figure 1.2. Then there is the possibility of having a variety of carbon nanotubes: Multi-walled carbon nanotubes (MWCNTs), or just a single walled carbon nanotubes (SWCNTs). SWCNTs were first observed in 1993 via scanning electron microscopy, forming bundles and occasionally isolated nanotubes could also be observed.⁶ Since then, a lot of research and experiments to separate these carbon nanotubes has been done (more than 200 papers)⁷ until 2010. A SWCNT can be defined by its chiral vector \mathbf{C}_h in Equation 1.1 and a theta angle (θ) in Equation 1.2.

$$\mathbf{C}_h = n\mathbf{a}_1 + m\mathbf{a}_2 \quad (1.1)$$

$$\theta = \arctan\left(\frac{\sqrt{3}m}{(m+2n)}\right) \quad (1.2)$$

Actually, the indices n and m describe the nanotube, as they refer to the number of unit vectors in the a_1 and a_2 direction in the honeycomb lattice containing C_h . Also, depending on the angle between the chiral vector and the a_1 direction, it is possible to have armchair, zigzag or chiral nanotubes as shown in Figure 1.3. The Table 1.1 summarizes the types of nanotubes according to n and m with their possible values of (θ) . Then, in Figure 1.2, C_h defines a chiral SWCNT with $n=7$ and $m=2$. In this figure the vector \mathbf{T} indicates the tube axis.

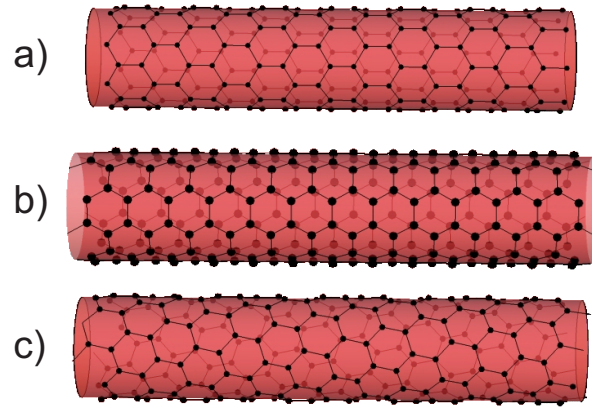


Figure 1.3: SWCNTs representations for a) zigzag nanotube (5,0), b) armchair nanotube (5,5), chiral nanotube (7,2). The SWCNT was generated using the Wolfram Demonstration Projects "Carbon Nanotubes"⁴.

Nanotube	Chiral vector	n,m indices
Zigzag	0°	$(n,0)$
Armchair	30°	(n,n)
Chiral	$0 < \theta < 30^\circ$	$(n,m), m \neq 0$

Table 1.1: Nanotube type according to n and m .

A carbon nanotube is also defined by its diameter with the relation between the nanotube's diameter and the n, m indices as Equation 1.3 indicates.

$$d_t = \frac{C_h}{\pi} = \frac{\sqrt{3}a_{C-C} \sqrt{m^2 + mn + n^2}}{\pi}, \quad (1.3)$$

where a_{C-C} is the nearest neighbour distance between two carbon atoms in the lattice, 1.421 Å⁸. Typically, the diameter of a SWCNT is between 0.4 and 3 nm⁹.

The (n,m) indices also determine the electronic response of the nanotube e.g. metallic or semiconducting. This has been predicted by electronic-band structure tight binding calculations¹⁰. If $(2n + m)/3$ is an integer the tubes are metallic, and otherwise semiconductin¹¹. This also implies that armchair nanotubes are always metallic while zigzag can be either metallic or semiconducting⁹.

1.2 Properties of SWCNTs

The properties of nanotubes will depend on the type of nanotube, according to its (n, m) values. Experimentally, the physical properties of nanotubes are measured considering their diameter distribution. These properties are remarkable because of the efficiency and potential that their implementations considering nano-applications¹². For instance, by combining their tensile properties as well as the electronic properties, nanotubes become candidates as molecular electronics components¹³.

1.2.1 Mechanical properties

Among the mechanical properties that are exhibited when forces are applied to a material are tensile strength, elongation, hardness, modulus of elasticity (Young's modulus) and fatigue limit¹⁴. All these features are tremendously well exhibited for carbon nanotubes because of the inter-atomic forces and the spatial arrangement of the carbon atoms¹⁵.

For the case of carbon nanotubes, the measurement of mechanical properties involves the use of the atomic force microscopy to measure the mechanical properties since the frequency modulation-atomic force microscope allows the measurement of conservative and non-conservative forces¹⁶.

The Young's modulus is a measure of the stiffness of a solid material¹⁷. It tells about the ability of the material to return to the original length after applying tension or compression. For

the case of carbon nanotubes, the Young's modulus can be obtained experimentally by measuring thermal vibrations using TEM¹⁸, this study has shown that the modulus increases when the nanotube's diameter decreases. Other methods involve the use of the atomic force microscopy to measure the mechanical properties since the frequency modulation-atomic force microscope allowed the measurement of conservative and non-conservative force¹⁶. Theoretically, with molecular dynamics approaches, non-orthogonal tight binding model and electronic energy-band theory, the Young's modulus is predicted to be 5.3 TPa in average^{19,20} which is 3.98 times higher than for diamond²¹.

1.2.2 Optical and electronic properties

The density of states (DOS) is a mathematical function that describes the number of states at a particular energy range that electrons are allowed to occupy²². With this concept it is possible to describe the electronic structure calculations of a material²³, that is, the allowed energies that the electron can have which are given as a function of the K-points from the first Brillouin zone of the reciprocal lattice²⁴. The optical properties of any material are governed by electronic interband transitions²⁵, as well as the electrical and electronic properties.

The DOS of suspended graphene is known for being zero at the Fermi level and its energy dispersion has six k points at the corners of the Brillouin zone (the valence π and conduction band π^* show degeneracy at those points), then the conduction and valence band meet and makes graphene a semiconductor with zero bandgap only on those points. The presence of a Dirac cone at each K-point is shown in Figure 1.4

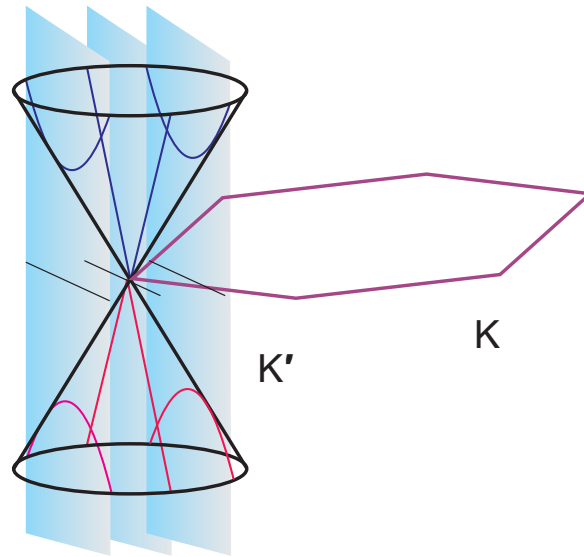


Figure 1.4: Zone folding axis method applied to graphene to obtain the DOS of SWCNTs.

The DOS of graphene has to be explained so that the DOS of SWCNT can be introduced. By setting some boundary conditions for SWCNT i.e. the cylindrical form of a graphene, the 1D band energy corresponding to SWCNTs can be obtained by cutting a cross section on that of graphene (the zone folding axis method)²⁶ as represented in Figure 1.4. Those cuts will be different depending on the diameter and chirality of the nanotube i.e. (n,m) indexes; semiconducting nanotubes with a diameter between 0.8 and 3 nm will have a bandgap of 0.2-0.9 eV, armchair nanotubes (n,n) will always be metallic²⁶.

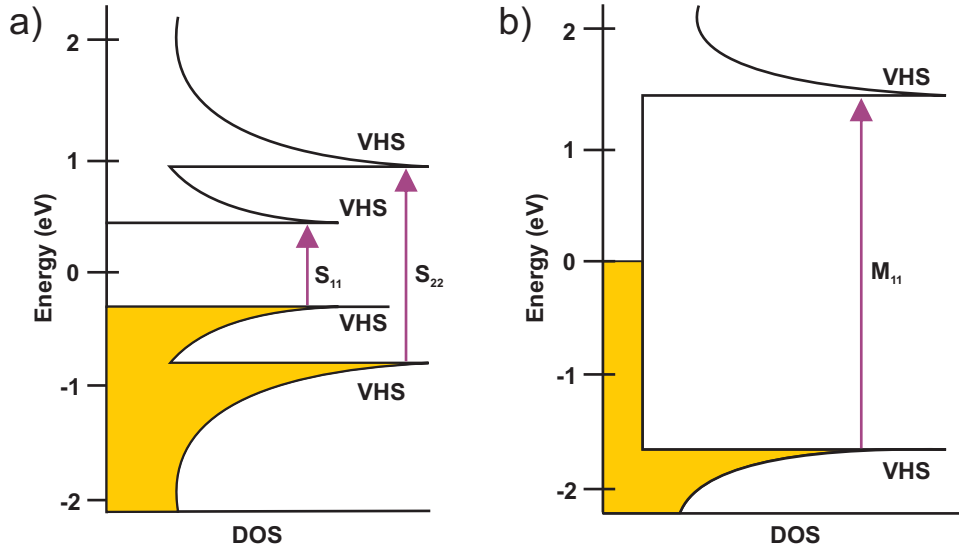


Figure 1.5: Representation of the DOS of a) semiconducting and b) metallic SWCNT. The optical transitions between the Van Hove singularities are also indicated.

As can be seen in Figure 1.5, the DOS related to this one dimensional material is not smooth. It increases and then decreases forming "spikes". These critical points are the Van Hove singularities (VHS) and are important for the optical absorption of the nanotubes as will be discussed later. Van Hove singularities which are present in one dimensional crystals at energies that are associated to a minima or maxima of energy²⁷. In other words, for 1D materials, the DOS diverges as the inverse of the square root of the energy $1/\sqrt{E(k)}$ close to band extrema. From dispersion relations one could analytically derive the position of the VHS²⁸.

Figure 1.5 also shows the optical transitions for a metallic and semiconducting carbon nanotube. The symmetric transitions between those singularities from the valence band to singularities in the conduction band are the only ones permitted²⁹. Optical transitions are established in the so called Kataura plot. A Kataura plot contains all the allowed electronic transitions with respect to the SWCNT diameter³⁰.

1.3 Synthesis of SWCNTs

The typical methods for which one can synthesize SWCNT include arc discharge, laser ablation method, chemical vapor deposition³¹ that can be either CoMoCAT[®] or high pressure carbon monoxide (HiPco[®]).

The arch discharge method uses two graphite electrodes that are placed in a space fill with an inert gas. The graphite anode contains a metal catalyst (like iron or cobalt) and powdered carbon precursor to synthesize SWCNTs in the form of soot. This method uses the electrical breakdown of a gas (arc discharge) to generate plasma which at high temperatures sublimates the carbon precursor. The carbon vapour drifts to the cathode where it cools down. The cathode is the deposit of the nanotubes³². In the laser ablation method there is a graphite target that just like in the arch discharge method, also contains the metal catalyst (usually cobalt or niquel)⁹. The vaporization of the material from this solid target is achieved thanks to laser pulses that heat the graphite that is placed in a argon atmosphere³³. A plasma plume is formed and then cools during its expansion. At this moment, carbon and catalyst metal atoms condense into larger structures³⁴.

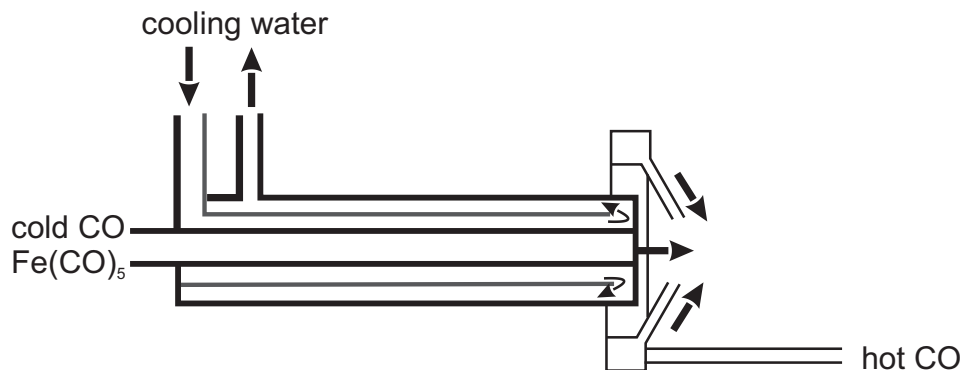


Figure 1.6: CO flow-tube reactor for high pressure carbon monoxide method. This scheme shows the water-cooled injector. Image adapted from Nikolaev et al.³⁵

The high pressure carbon monoxide (HiPco[®]) method consists on having carbon monoxide at temperatures of 800 -1000 °C and pressures of 1–10 atm, as the raw material and iron pentacarbonyl (Fe(CO)₅) as the catalyst precursor in a continuous flow gas³⁵. The precursor decomposes and leads to the formation of metal particle clusters. Then the nucleation process takes place

and finally the growing of the carbon nanotubes. Solid carbon is produced by carbon monoxide disproportionation³⁵, hot and cold carbon are in the turbulent flow regime (Figure 1.6). In the last years, other sophisticated methods are being evolved³⁶. It is expected that depending on the method used, one can end up with a preferred type of pure carbon nanotubes (enriched SWCNT). For this research project, SWCNT HiPco[®] enriched 99 percent with small diameters³⁷ will be used.

1.4 Bundles in SWCNTs and their dispersion

The synthesis of SWCNTs results in an entanglement of nanotubes which leads to bundle formation³⁸. Van der Waals forces describe the attraction with induced or permanent dipole moments. Van der Waals interactions are present between the nearest nanotube neighbours. They dominate the system and make the nanotubes parallel every time is possible so that crystalline ropes are formed³⁹.

The debundling and dispersion of SWCNTs is important since their properties are expressed when they are individually dispersed⁴⁰. There are basically two approaches to disperse the carbon nanotubes: mechanically and chemically.

The mechanical approach includes for instance sonication, or ultrasonication and their derivatives (bath, tip, probe etc.) Ultrasonication is used for homogenization, deagglomeration of liquids. The working principle consists on producing sound waves that are transmitted in the solution to create high and low pressure cycles that will depend on the frequency applied. The generated shear forces are sufficiently enough to overcome the Van der Waals interactions between the carbon nanotubes⁴⁰.

The chemical approach alters the surface energy of the solids in a covalent and non-covalent manner⁴¹. Covalent modification induces defects in the walls of the carbon nanotubes⁴². On the other hand, non-covalent stabilization is supposed to maintain the properties of the SWCNTs dispersions⁴³, this includes the dispersion of the nanotubes in surfactants⁴⁴, polymers and organic solvents⁴⁵.

The chemistry of the nanotubes allows them to be dispersed in solvents and polymer solutions like polyacrylonitrile (PAN) and dimethyl sulfoxide (DMSO), N,N-dimethylacetamide (DMAc), N-dimethylformamide (DMF)⁴⁵. The dispersion in this last solvent has been reported before⁴⁶.

DMF is a very polar solvent with the chemical formula $(\text{CH}_3)_2\text{NCOH}$, its Lewis structure is represented in Figure 1.7 for the molecule. The National Institute of Standards and Technology (NIST) suggests the use of N-dimethylformamide (DMF) as the solvent for the SWCNTs dispersion.

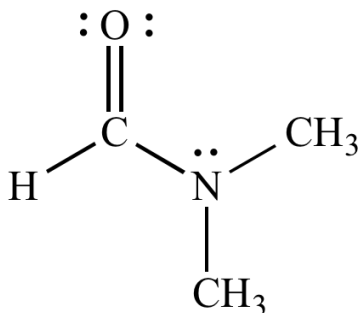


Figure 1.7: It has three single covalent bonds represented by one line, a double bond represented by two lines. The pair of dots represents a pair of unshared electrons.

For the bundles to be untangled and well dispersed in a solvent, they have to overcome the cohesive energy, that is, the energy required to break joint atoms⁴⁷. Solvents like water need the addition of a surfactant for the total dispersion.

Surfactants are amphiphilic molecules which means that they have a polar head (hydrophilic) and a non polar tail (hydrophobic). There exist different types depending on the charge of the head and tail, for example: cationic (CTAB), anionic (SDBS, SDS), nonionic and zwitterionic. As mentioned before, the surfactant is adsorbed, which means that the atoms of the surfactant will adhere to the surface of the nanotubes. The self-accumulation into supramolecular structures is also an important feature of surfactants. For instance, the driving force between an ionic surfactant and a charged nanotube will be the Coulombic attraction⁴¹. But, the removal of the surfactant might be necessary if one would like to study the intrinsic properties of the nanotube or use the nanotubes for an specific application⁴⁸.

1.5 Graphite Intercalation Compounds

Graphite intercalation compounds (GICs) are complex materials that are formed by placing heteroatoms or molecules of a different chemical species between the layers of carbon⁴⁹. In GICs, the intercalant species donate electrons or accept electrons from the graphite layers.⁵⁰ Some of the intercalation methods include the two-zone vapour transport technique, the liquid intercalation method, the electrochemical method and cointercalation technique⁵⁰.

GICs can have different stages depending on the number of carbon layers between nearest intercalant layers⁵¹. GIC stage I will refer as one graphene layer that is covered by adjacent intercalant layers as in Figure 1.8 a). Similarly, stage II indicates that two graphene layers are covered by adjacent intercalant layers as in Figure 1.8 b).

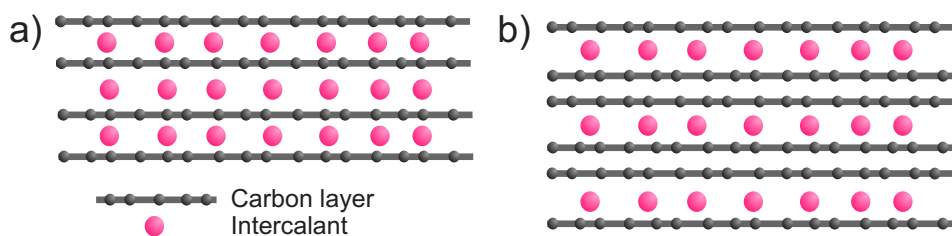


Figure 1.8: Schematic illustration of GIC a) stage I and b) stage II.

By means of heating, exfoliation of GICs can occur⁵². The exfoliation of GICs can lead to flexible graphite⁵³, sheets of graphene oxide by exposure of water vapour⁵⁴. Also, by involving chemical treatments of thermal exfoliation it is possible to reduce graphene oxide⁵⁵. Figure 1.9 represents a typical process for an exfoliation process from GIC.

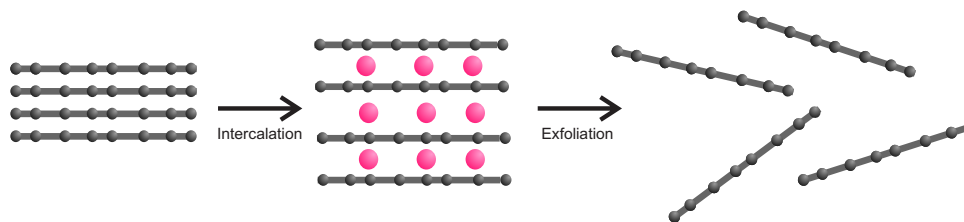


Figure 1.9: Exfoliation process starting from GIC.

Chapter 2

Motivation

*If you don't know where you are going any road
can take you there.*

Lewis Carroll

The large scale production of the nanotubes include having impurities which will interfere with the desirable/expected properties⁵⁶, so a process of purification is required. But also, in order to facilitate the manipulation of SWCNTs for their chemical and physical characterization, the correct solubility of the carbon nanotubes in an aqueous media is required⁵⁷. By individualizing the SWCNTs, it is possible to take advantage of their intrinsic properties. The current SWCNTs individualization techniques include processes that tend to damage the structure of the carbon nanotube. e.g. long centrifugation time.

In the same manner that it is possible to obtain graphene oxide from the exfoliation of GICs⁵⁵, a chemical exfoliation consisting on GICs with the SWCNTs will be intended. For this case, two alkali metals will be the electron donors: potassium and sodium. These two will be intercalated within the bundles of the SWCNT. The intercalation compounds with SWCNTs has been successfully done before with potassium, caesium, rubidium and iodine⁵⁸⁻⁶¹. Coulomb explosion has already been tested for the individualization of SWCNTs from their bundles⁶². It is expected that a Coulombic repulsion is achieved since the nanotubes will be negatively charged (as they will become electron acceptors). This way the carbon nanotubes can separate until their individualization. On the other hand, the use of surfactants allows the functionalization of the sidewalls of the nanotubes and then it is hard to remove the surfactant from the nanotube. The decision

to use DMF (organic solvent) instead of any surfactant lies mainly in two reasons. First, this organic solvent has been tested before in previous research giving successful results (in terms of dispersion). Second, some polymers interact more than the particles of a surfactant, so the solubility increases.

In this research project it is propose the characterization of individualized HiPco[®] SWCNTs looking to preserve their pristine properties by cooling, a simple chemical method that consists on a charge transfer donor mechanism from an alkali metal dispersion in an organic solvent followed by a sonication process. The characterization techniques can help to understand the results form the exfoliation and dispersion. Also, it will be possible to make a quantitative analysis on the type of nanotubes that resulted, specially according to the RBM frequency analysis of Raman spectra.

Chapter 3

Methodology

If I had a world of my own, everything would be nonsense. Nothing would be what it is, because everything would be what it isn't. And contrary wise, what is, it wouldn't be. And what it wouldn't be, it would. You see?

Lewis Carroll

3.1 Synthesis

3.1.1 Intercalation compounds

The Unidym HiPco[®] SWCNT were purchased for the experiment. They passed through a drying process (heat at constant temperature) to remove most of water molecules as possible. This was necessary because they were about to be intercalated with high reactive alkali metals and the conditions in the glove box needed to remain with 0.1 ppm of oxygen and 0.1 ppm of water.



Figure 3.1: Diagram for the intercalation compounds synthesis

The intercalation compounds were synthesized in the glove box. Figure 3.1 shows a flux diagram of the synthesis process. The alkali metals and the SWCNT were accurately weighed to ensure the proportions according to the intercalation compound stage. The resulting intercalation compounds were the first stage alkali metal donor compounds KC_8 and NaC_8 , and the second stage alkali metal donor compound KC_{24} . In order to complete the exfoliation, the samples were always at a constant temperature of 200 °C.

3.1.2 Dispersion in the solvent

The dispersion of the GICs were done in a very dry DMF solvent that was previously freeze pumped and distillate. Also, molecular sieves were added. For each 0.1 milligram of the intercalation compound, 1 millilitre of the solvent was added. Notice that the density of DMF is 0.944 g/ml. In order to achieve an uniform dispersion, tip sonication at five revolutions per minute was performed during five minutes.

3.2 Scanning Electron Microscopy

SEM is a frequently used characterization technique. A 3D like-image of the surfaces of organic and inorganic nanometric to micrometric scale can be obtained⁶³.

Goldstein et al. expand on the theory behind the SEM, the instrumentation used and the mechanism to generate the image⁶³. Basically, a SEM system includes a lens system, the source of electrons and its collector, the visual and recording cathode ray tubes and the electronics associated that allows to communicate all the system. The principle behind this technique is the interaction between a beam of electrons and the surface of the sample. That beam of electrons is generated thanks to a process called thermionic emission in which the electrons overcome the

work function and are ejected from a cathode (e.g. tungsten filament). A grid cap is enveloping the filament and acting as a negative bias with respect to the cathode, that in combination with the acceleration of electrons to the anode (electric field as gun configuration) finally causes the electrons to converge to a crossover point. Condenser and objective lenses are also placed to demagnify the electron image at the crossover and obtain the final electron probe. Electron magnetic lenses are also used to focus the electron beam because of the electromagnetic field of the lens on the moving electrons (Figure 3.2). The column needs to be in high vacuum such that no air molecules interfere with the electron probe and they can finally arrive to the sample.

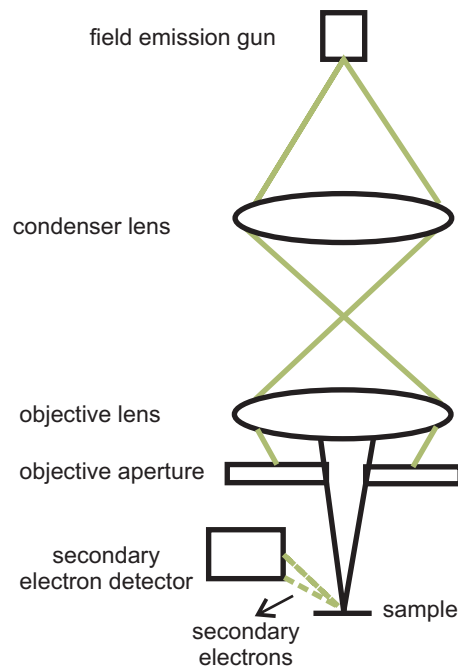


Figure 3.2: SEM scheme showing the main elements.

As a result of the initial voltage and consequently the heating of the filament, there is a current density which is a combination, with other parameters that determines the brightness for the formation of the final image. Parameters such as the applied voltage, aperture size, current, no defects in lenses, correct sample preparation will yield to a good resolution in the final image. The interaction between the electron probe and the sample result in secondary, backscattered

electrons and characteristic x-ray lines and other. They can be recorded depending on the selected detector. If one wants to get information about the morphology of the sample, the detector selected should be that of the secondary electrons since those electrons are generated from the collisions between the incoming electrons and loosely bonded outer electrons of the sample. The SEM images presented in this research were obtained with FEI-HELIOS NanoLab 600i FIB equipment with 10 kV as the applied voltage.

3.3 Atomic Force Microscopy

Scanning probe microscopy (SPM) covers the imaging and measurement of surfaces at molecular and atomic levels⁶⁴ on nanometer length scales⁶⁵. Scanning electron microscopy (SEM) and atomic force microscopy (AFM) cover precisely this field. SEM was first invented in 1931 and it works on the principle of quantum tunnelling so that only conducting or semiconducting surfaces can be studied. Later on, in 1986 the AFM gave the possibility of working with any kind of sample (including insulators).

"AFM combines force measurement with high spatial resolution."⁶⁶ The parts involved in this technique are a sharp conductive or tip with often less than 100 Å in diameter and 2 μm in length, a cantilever, a laser beam, a detector (photodiode) and a piezoelectric stage. The force between the tip and the surface of the material make the cantilever deflect as well as the laser beam pointing towards the tip as indicated in Figure 3.3. The surface is scanned by the tip thanks to a piezoelectric that expands and contracts proportionally to an applied voltage and uses a feedback loop to readjust parameter and finally get an image of the surface. That information is received by a photodiode that later on will translate the signal into a e.g. topographic image. The principle relies on recording electrostatic, magnetic forces and interatomic interaction between the tip and the surface of the sample.⁶⁷

The AFM uses a cantilever with a spring constant which is weaker than the equivalent spring between atoms. This way, the tip can "image" conducting and non conducting samples at atomic resolution⁶⁷. This statement is in accordance with Hook's law (Equation 3.1) where k is the cantilever and Δz is position of the cantilever from its equilibrium position⁶⁸.

$$F = k\Delta z \quad (3.1)$$

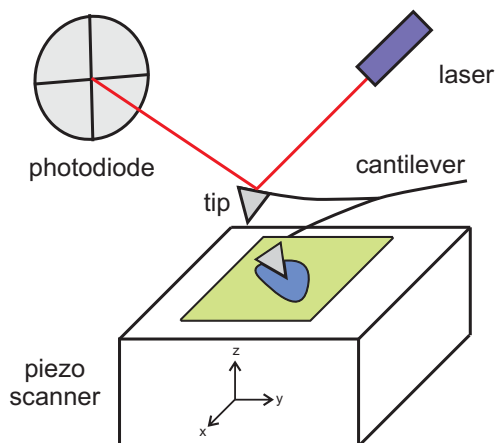


Figure 3.3: AFM scheme showing the main parts.

AFM measurement has a series of modes including tapping, contact and non-contact mode. The contact mode is when the tip is touching the surface and the repulsive forces are measured. Here, the deflection of the cantilever is kept constant. The image is the result of the movement of the piezoelectric stage.

There is a contact and a non-contact mode. The contact mode is when the interaction between the tip and the sample is dominated by short range interatomic forces. On the other hand, the non-contact mode is when those interactions are dominated by longer range forces (e.g. magnetic, electrostatic and attractive van der Waals forces) that are appreciable when the tip is moved away by 10-100 nm.

For the AFM measurements, the sample was placed in a silicon dioxide wafer. The AFM images were obtained with a Bruker ICON Cover Assy REVC Dimension equipment.

3.4 Raman Spectroscopy

Spectroscopy is the study of the interaction of electromagnetic waves with matter.⁶⁹ An incoming light source with $\hbar\omega_S$ is absorbed by the sample and then a light with energy $\hbar\omega_L$ is emitted, this is known as light scattering.⁷⁰ The different types of light scattering includes Rayleigh, Stokes and anti Stokes scattering as shown in Figure 3.4. But only for the last two, the scattering is

said to be inelastic $\omega_S \neq \omega_L$ and are part of Raman scattering. Stokes and anti Stokes inelastic scattering are two-photon events involving the simultaneous annihilation of the incident photon and the creation of a scattered photon⁷¹.

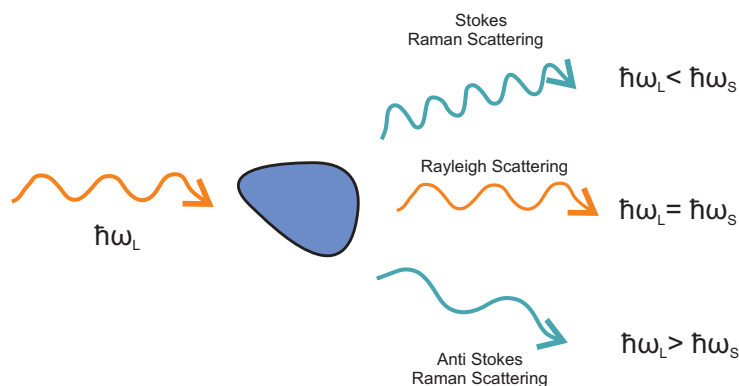


Figure 3.4: Scheme for the scattering of light including Rayleigh, Stokes and Anti-Stokes scattering.

In 1928, it was the Indian physicist V.C. Raman who discovered and described the phenomena called after his name⁷². He and his colleague K.S. Krishnan referred to Raman scattering as a "new type of radiation". Stokes Raman scattering is when the incident photons have less energy than the frequency due to the interaction of the radiation with the molecule which results in an upward transition. On the other hand, anti Stokes Raman scattering results in a downward transition⁷³ where the incident photons has more energy than the scattered ones. This is represented in Figure 3.4.

The first-order Raman scattering involves a single quantum of excitation in the medium⁷⁴ known as phonon. There are some selection rules for a Raman process to take place, this includes energy and momentum conservation, crystal and excitations symmetries. Considering the incoming monochromatic light with frequency ω_L and propagation vector \mathbf{k}_L , after the inelastic process with scattering frequency ω and propagation vector \mathbf{k} , the outgoing scattered light will have the frequency ω_S and propagation vector \mathbf{k}_S . Then, Equation 3.2 follows the first law of thermodynamics: energy conservation. And it follows the same for the wave vector (Equation 3.3).

$$\omega_L = \omega_S + \omega, \quad (3.2)$$

$$\mathbf{k}_L = \mathbf{k}_S + \mathbf{k}, \quad (3.3)$$

A crystal with perfect translation symmetry has its crystal momentum \mathbf{q} to label the elementary excitations, and also momentum conservation. The elementary excitations can be represented by a dispersion relation in which a value of $\omega_{\mathbf{q}}$ belongs to each value of \mathbf{q} ²². When a single elementary excitation is involved (first-order scattering process), the scattering wave vector is equal to the wave vector of the excitation ($\mathbf{k} = \mathbf{q}$) and similarly occurs with the frequency ω , $\omega = \omega_{\mathbf{q}}$. For higher-order scattering processes, the sum of two or more frequencies of elementary excitations is ω and the total wave vector is \mathbf{q} . In this context, the concept of elementary excitation refers to phonons. In the same way that photons are the unit energy of electromagnetic waves, phonons are the unit of vibrational energy that emerges from oscillating atoms within a crystal.

Now, Equation 3.2 becomes Equation 3.4 and Equation 3.3 turns into Equation 3.5. Figure 3.5 shows a scheme for the momentum conservation for Raman scattering.

$$\omega_L = \omega_S + \omega_{\mathbf{q}}, \quad (3.4)$$

$$\mathbf{k}_L = \mathbf{k}_S + \mathbf{q}, \quad (3.5)$$

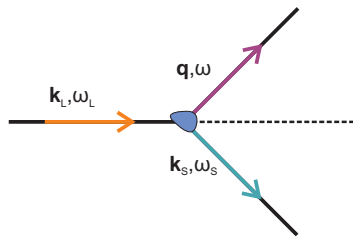


Figure 3.5: Momentum conservation in an inelastic scattering process according to Equations 3.4 and 3.5.

3.4.1 The Raman spectrometer

Although the first Raman equipment used a beam of the sunlight as the source of radiation (with the help of a telescope objective)⁷², later if a more intense light source was needed and the implementation of lasers was introduced to modern Raman spectrometers. The Raman spectrometer consists basically of three parts, the laser source, a spectrometer as the detector and a set of mirrors and filters to focus and collect the light. As indicated in Figure 3.6, the incoming light represented with red color line, travels through a band pass filter to pass only the laser line and a dichroic mirror (Rayleigh filter). Later on, the light (that has been focused and -red) is reflected by a mirror and enters to a system of lenses (optical microscope) to be scattered by the sample. The optics in the microscope will collect the scattered light and go directly to a focusing mirror and a long pass filter to the grating through which it is dispersed. The dispersed light is finally focused onto the detector. The shift in frequency of the scattered light in comparison with the initial frequency is measured with a Raman spectrometer⁷⁵. Each ω_S is a frequency that belongs to an internal transition (electronic, vibrational, or rotational) of the constituent molecules⁷⁶. This is the reason why each Raman spectrum provides a "fingerprint" of a molecule/species and is considered a useful technique to identify a material⁷⁶.

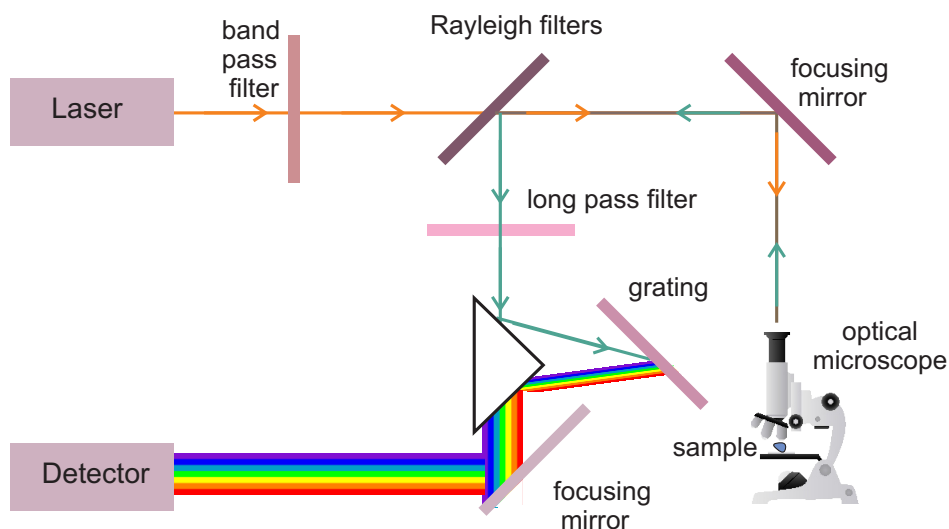


Figure 3.6: Scheme of a simplified Raman spectrometer. The basic constituents are shown as well as the path of the incoming light (orange) and scattered light (blue).

3.4.2 Origin of the characteristic Raman modes for SWCNTs

Raman Spectroscopy is very popular for the characterization of carbon based nanomaterials. In the case of SWCNTs the following modes are present: Radial breathing mode (RBM), D mode (also known as the disorder-induced band⁷⁷) at 1350 cm^{-1} , G^- and G^+ line and finally the G' mode at around 2700 cm^{-1} .

The Raman scattering processes that give rise to the modes for graphene are summarized in the Figure 3.7, and are similar to that of carbon nanotubes because of the theoretical description of a carbon nanotube from a graphene layer. Because of a electron-phonon coupling interaction, the G mode is originated⁷⁸, as shown in Figure 3.7 a). The electron is scattered by a phonon. The electron-hole pair recombines and emits a photon that is red shifted by the amount of energy given to the phonon⁷⁹. For SWCNTs, this mode splits into G^- and G^+ lines⁸⁰.

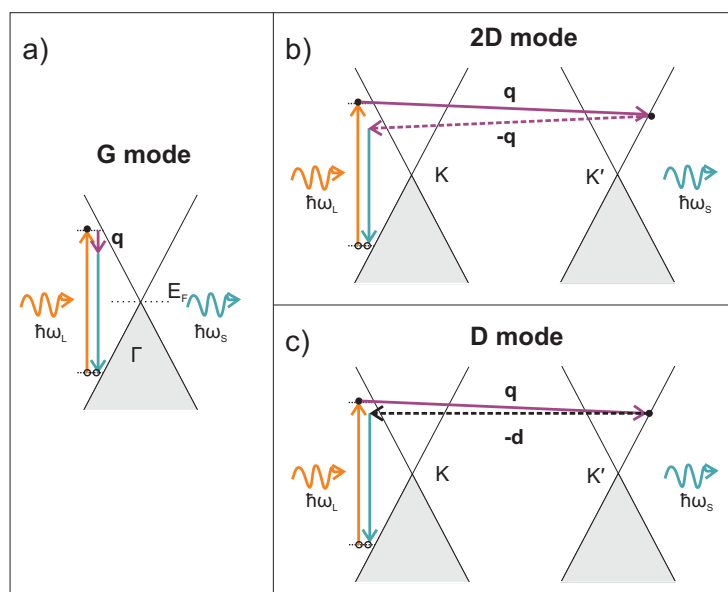


Figure 3.7: Scheme for the Raman scattering processes that give rise to the a) G b) 2D and c) D mode of graphene.

RBM is a special feature of the SWCNTs. They correspond to the carbon atoms vibrations in the radial direction⁸¹ as shown in Figure 3.8, and its frequency belongs to a specific diameter⁸². The range in which the RBM occurs is between 150 and 300 cm^{-1} ⁸³.

The origin of the D and 2D line is a double resonant process^{84,85}. The 2D mode originates from the in-plane breathing-like mode of the carbon ring. An electron-hole pair is created by an incident photon near the K point. The electron is inelastically scattered by a phonon to the K' point. Following the energy and momentum conservation, the electron must scatter back by a second phonon to K before recombining with the hole. The 2D mode in graphene is commonly used as G' line for carbon nanotubes⁸⁶. The origin of the D mode requires a defect for the momentum conservation. The electron is inelastically scattered by an phonon to the K' point and then is elastically back-scattered to the K point by a defect⁸⁷.

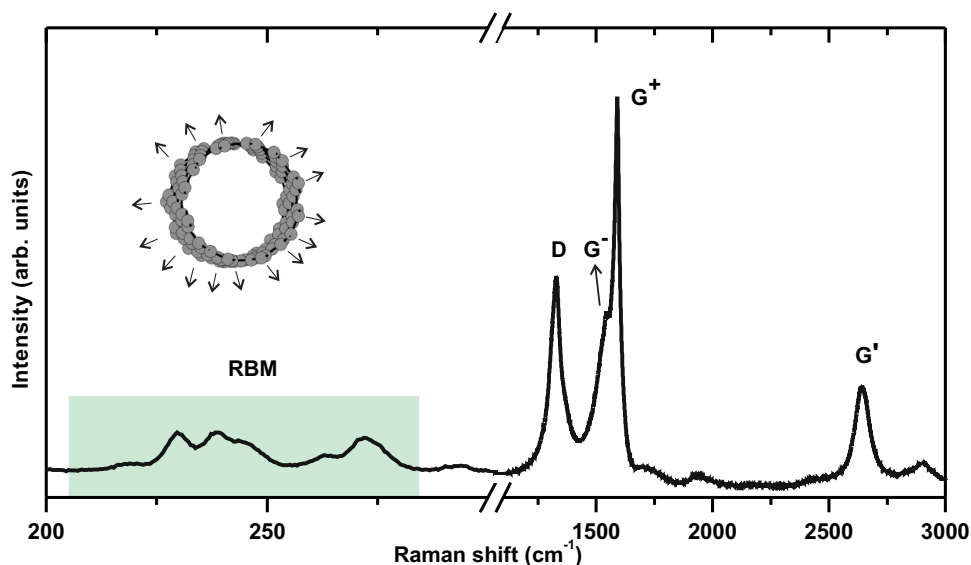


Figure 3.8: Typical Raman spectrum of SWCNTs presenting the RBM peaks, G⁻, G⁺ and G' lines. Inset is shown the like-breathing motion of a carbon nanotube.

The linewidths of the different Raman modes depend on the physical origin of the scattering processes. For second Raman processes, the linewidths in sp² carbon materials are broader than for first order Raman G mode in graphite⁸⁸. The lineshape of the G⁻ line has been used to identify whether the nanotubes are metallic or semiconducting. The presence of metallic nanotubes makes a broader shape of the G⁻ line in comparison with that of the semiconducting nanotubes (which is more narrow); this broad shape for metallic nanotubes occurs because of the the presence of free electrons⁸⁹. The broader shape is very common for n-doped graphite

intercalation compounds (GICs)⁹⁰.

The Raman spectrometry characterization of the SWCNTs in this project was performed in Horiba Scientific - LabRAM Aramis Raman spectrometer using a laser of 532 nm. The samples were placed in a silicon dioxide wafer so that the characteristic peak for silicon at 520 cm^{-1} could be observed, and the calibration of the spectrum can be perfectly done. Only the pristine powder: HiPco[®] was placed in a carbon tape. It is very common to place powder samples on a carbon tape which have a thick conductive adhesive, this helps to stick the powder sample and makes possible the SEM imaging since it ensures also the conductivity that is required to obtain the SEM imaging correctly.

Chapter 4

Results & Discussion

Every picture tells a story. Sometimes we don't like the ending. Sometimes we don't understand it.

Lewis Carroll

As mentioned before in the introduction, the as-synthesized SWCNTs tend to aggregate into bundles to decrease their surface energy⁹¹. In the SEM image (Figure 4.1) it is possible to actually see the bundles. The length of SWCNTs has a size in order of microns. There is also the presence of some carbon nanotubes ropes dangling from the bundles. The bundles are still noticeable when they were dispersed in DMF as shown in the AFM image in Figure 4.2. The contact AFM mode generated an image in which it is found a maximum height of 9.13 nm. The most bright spots that correspond to higher height in the sample can be attributed to the presence of big bundles like the ones that are seen in the SEM image (Figure 4.1). As more nanotubes tangle to form a bundle, more height is expected.

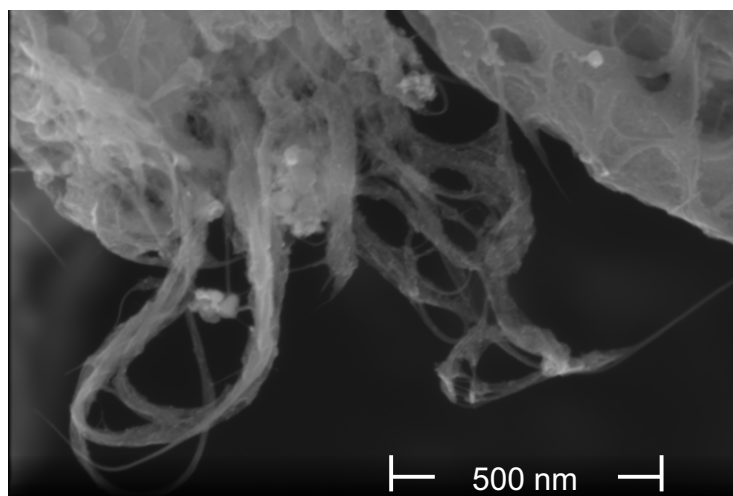


Figure 4.1: SEM image of the HiPco[®] SWCNTs in powder. The sample was placed on a carbon tape.

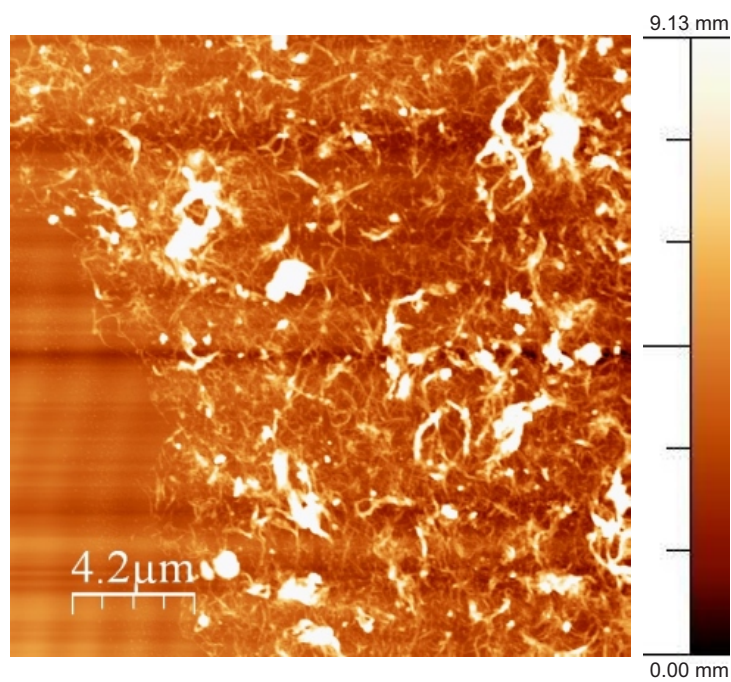


Figure 4.2: AFM image of the HiPco[®] SWCNTs dispersed in DMF.

Besides having AFM and SEM images to actually see the morphology of the HiPco[®] SWCNTs, with the Raman spectrum shown in Figure 4.3 the presence of SWCNTs is undeniable because the characteristic modes are present: RBM, D line, G⁻ and G⁺ line and finally the G' line. In the RBM region highlighted in Figure 4.3 there are at least eight peaks present (at a certain RBM frequency), this indicates the presence of at least eight types of nanotubes with different diameters (therefore different chirality according to 1.3).

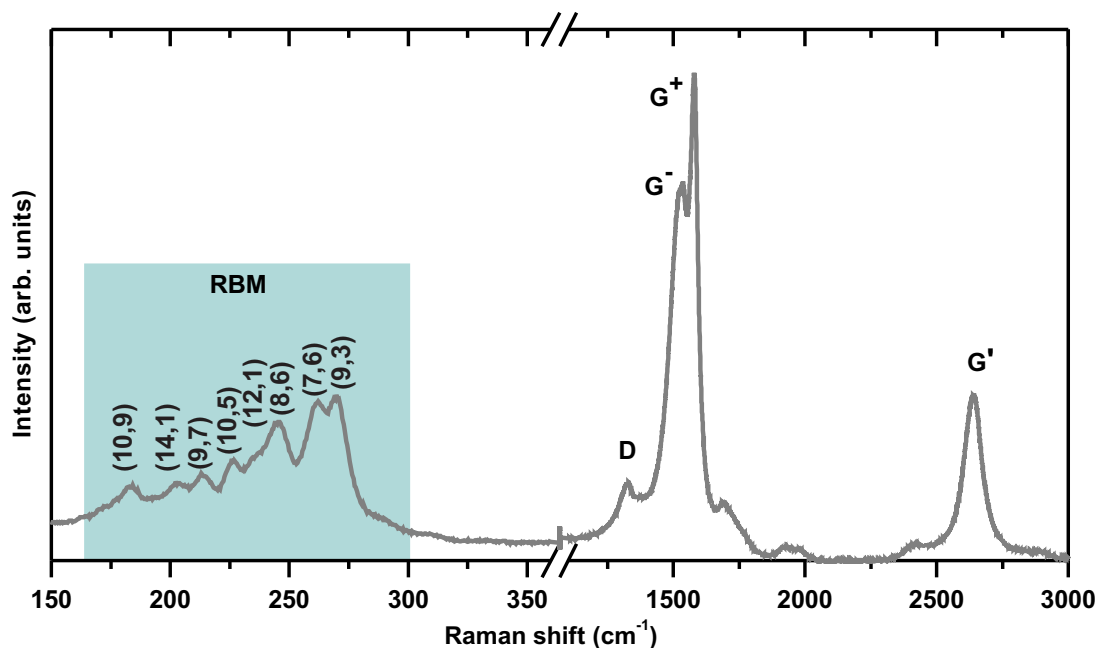


Figure 4.3: Raman spectrum of the pristine HiPco[®] SWCNTs taken with a 532 nm excitation laser. The characteristic peaks are present: RBM, D, G⁻, G⁺ and G' lines.

The assignment of the RBMs frequency was done by comparing the experimental frequency of the RBMs with that of the tables presented by Maultzsch et al.⁹² even though they suggest that the assignment of the RBM frequencies cannot be done just by purely looking at their frequency in the Raman spectrum. They mention that the effect of the solvent used to disperse the nanotubes and the excitation energy of the laser changes the final outcome. Moreover, the relationship between the diameter and the RBM frequency also varies with those parameters. For the proper and accurately assignment, an experimental Kataura plot should be constructed with

the data from a Resonance Raman Spectroscopy. The important point that will be discussed in this analysis is the absence or appearance of RBMs depending on the experiments performed (Figure 4.4). Table 4.1 indicates the assignment of the indices n and m according to the RBMs frequency observed in the spectrum of the pristine sample (Figure 4.3) and compared with that in Table I in reference⁹². The diameter of the nanotubes lies in the range of 8-12.9 Å which agrees with the range of HiPco[®] SWCNTs (according to the specification sheet of the product).

RBM ω (cm ⁻¹)	RBM ω reference ⁹² (cm ⁻¹)	Diameter (Å)	n	m
184.21	185	12.9	10	9
202.86	207	11.38	14	1
212.81	215	10.88	9	7
226.39	225	10.36	10	5
235.31	237	9.82	12	1
245.57	243	9.53	8	6
262.26	261	8.83	7	6
270.65	272	8.47	9	3

Table 4.1: Experimental RBM frequency and reference RBM frequency (ω) and the corresponding assignment of diameter and (n,m) indices for pristine SWCNTs

The D line of the pristine material appears at around 1324.75 cm⁻¹ while in literature the D line for graphite is reported to appear at 1350 cm⁻¹⁹³. It has been reported that for nanotubes, the frequency of the D line is smaller than for that of graphite⁹⁴. This mode is dispersive which means that its frequency will change depending on the photon excitation energy⁹³.

Typically, the G line has two components: G⁻ at 1570 cm⁻¹ and G⁺ at 1590 cm⁻¹. Figure 4.3 show the G⁻ line at around 1530.87 cm⁻¹ and G⁺ line at around 1577.91 cm⁻¹. The lineshape of this G⁻ band suggests the presence of semiconducting nanotubes since for metallic nanotubes, the peak is broadened because of the presence of free electrons⁸⁹. This is in agreement with the nanotube assignment in Table 4.1 since six out of eight nanotubes resulted semiconducting.

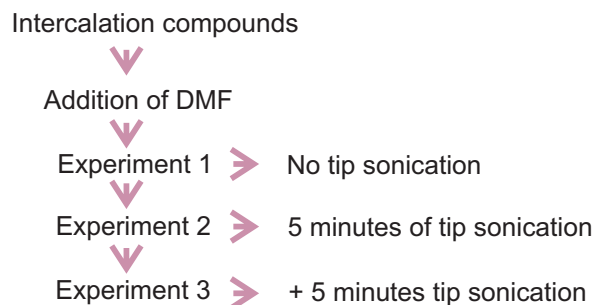


Figure 4.4: Diagram flow describing the three experiments that were carried out.

Afterwards, the synthesis of the intercalation compounds took place as well as their dispersion in DMF. In total, three experiments were carried out. Figure 4.4 shows a diagram flow indicating the processes that lead to the three experiments for this research project. The Experiment 1 consisted only in adding DMF to the intercalation compounds (no tip sonication was applied). As can be seen in Figure 4.6, the color of the sample turned black immediately after the dispersion in the solvent. This suggests, at first glance, the strong affinity of the solvent with the intercalation compounds. In Figure 4.6 a), from left to right, the NaC_8 , KC_{24} , KC_8 and the SWCNTs in DMF go from black color to less dark and finally the sample that was not intercalated with alkali metal, the nanotubes powder is sedimented at the bottom. With this, it might be correct to say that the intercalation compound have more solubility in DMF than HiPco[®] SWCNTs in DMF.

Other studies have shown that the potassium atom is not expected to be inside the tube but in the interstitial sites of bundles^{60,61}, and occupying the triangle voids between three adjacent tubes, and for K saturated, three potassium atoms per cavity⁵⁸, as indicated in Figure 4.5. The charge transfer of the alkali metals to the carbon nanotubes causes a repulsion between the nanotubes. Therefore they repel from each other, causing a better dispersion of the nanotubes in the solvent. The solubility increases for the intercalation compounds.

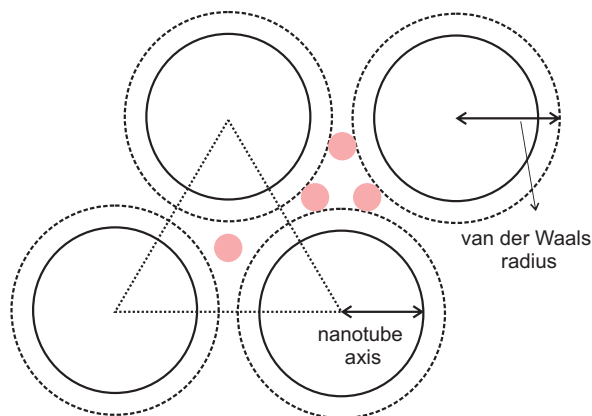


Figure 4.5: Model for the K atoms position in a SWCNTs bundle proposed by Duclaux et al.⁵⁸.

The Experiment 2 consisted on making the tip sonication during five minutes at five revolutions per minute to the samples of Experiment 1. The samples from Experiment 2 were taken to the silicon dioxide wafer immediately for their respectively analysis. Finally, Experiment 3 consisted on making another tip sonication for another five minutes. The image shown in (Figure 4.6 b)). The samples were taken from the first two thirds of the vial to the silicon dioxide wafer. From left to right, the vial containing NaC_8 , KC_{24} , KC_8 still looked stabilized (the black color remained), and the SWCNTs in DMF is the only sample that looked sedimented. Again, it is found more solubility due to the intercalation compounds.

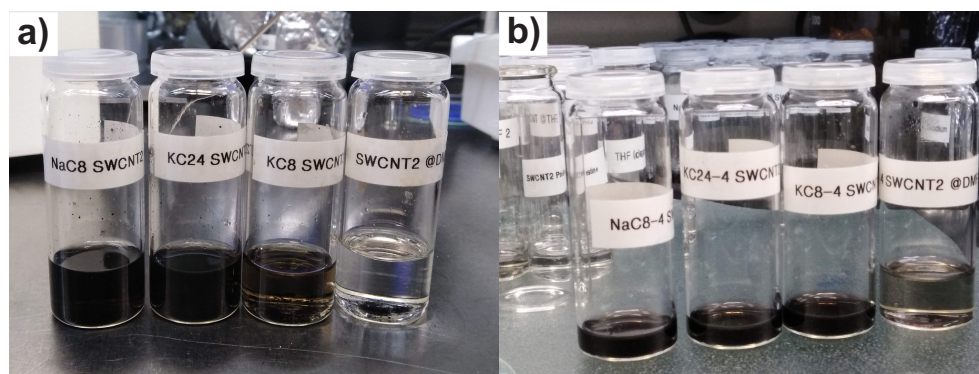


Figure 4.6: Image of the intercalation compounds and pristine dispersed in DMF with a) no tip sonication (Experiment 1) and b) after ten minutes of tip sonication and twenty four hours of rest (Experiment 3).

The Raman spectrum of the samples from Experiment 1 is shown in Figure 4.7. By just looking at the position of the D line, a sustainable shift of the frequency of this line is not detected for the intercalation compounds. The D mode needs the presence of a defect for momentum conservation. Having sodium or potassium as the intercalant and at any stage does not make a difference for this mode. This is equivalent to saying that the disorder caused by the three samples is the same.

The lineshape of the G' line from Experiment 1 is different from that of pristine SWCNTs; the broadness of the peak indicates the presence of metallic behaviour even though the assignment of RBMs frequencies in Table 4.2 indicates the presence of semiconducting nanotubes. But, Pichler et al. showed that SWCNTs turn metallic because of the potassium intercalated bundles of SWCNTs⁵⁹. This might be the reason why the lineshape of the G' indicates metallic nanotubes.

The G' line has a different shape for each intercalation compound even comparing them with the pristine sample. Other Raman studies from graphene layers in GICs show a dependency of the frequency of the 2D (G') line with high stages of the intercalation compound (higher than II), in which there is a downshift of the 2D (G') line when the stage number of the intercalation compound increases⁹⁵. However, in this case for SWCNTs, the opposite is observed (Figure 4.7). The intensity of the G' line does increase for higher stage GIC (KC₂₄).

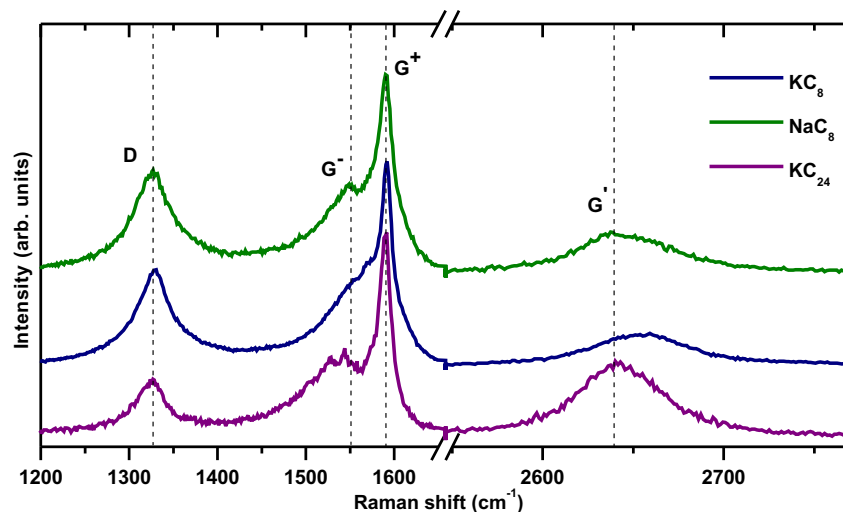


Figure 4.7: Raman spectra taken with a 532 nm excitation laser, showing the G^- , G^+ and G' lines of the GICs from Experiment 1.

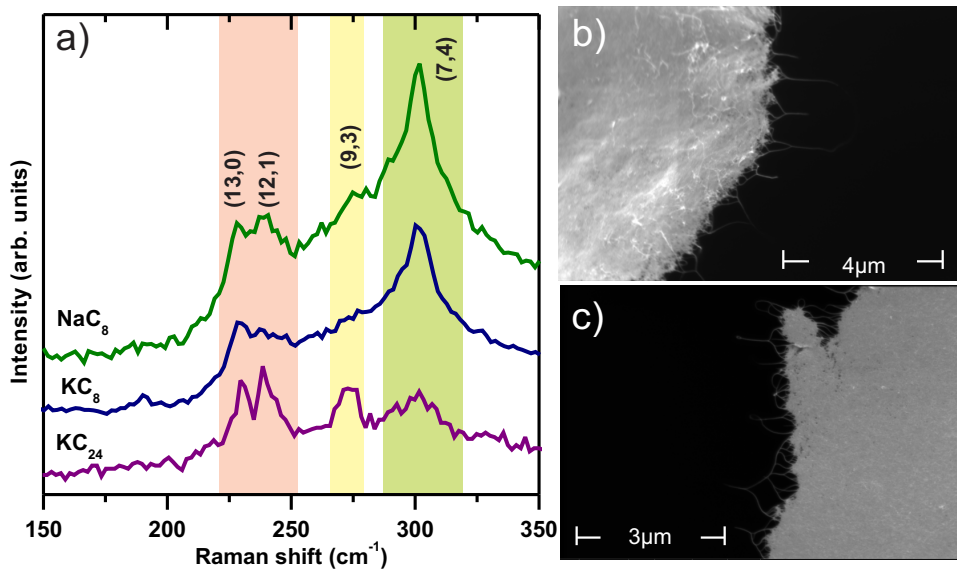


Figure 4.8: GICs from Experiment 1. a) Raman spectra taken with a 532 nm excitation laser of the RBM region b) SEM image of KC_{24} , c) SEM image of NaC_8 .

RBM ω (cm ⁻¹)	RBM ω reference ⁹² (cm ⁻¹)	Diameter (Å)	n	m
228.51	229	10.18	13	0
238.58	237	9.82	12	1
273.83	272	8.47	9	3
301.71	302	7.55	7	4

Table 4.2: Experimental RBM frequency and reference RBM frequency (ω) with the corresponding assignment of diameter and (n,m) indices from Experiment 1.

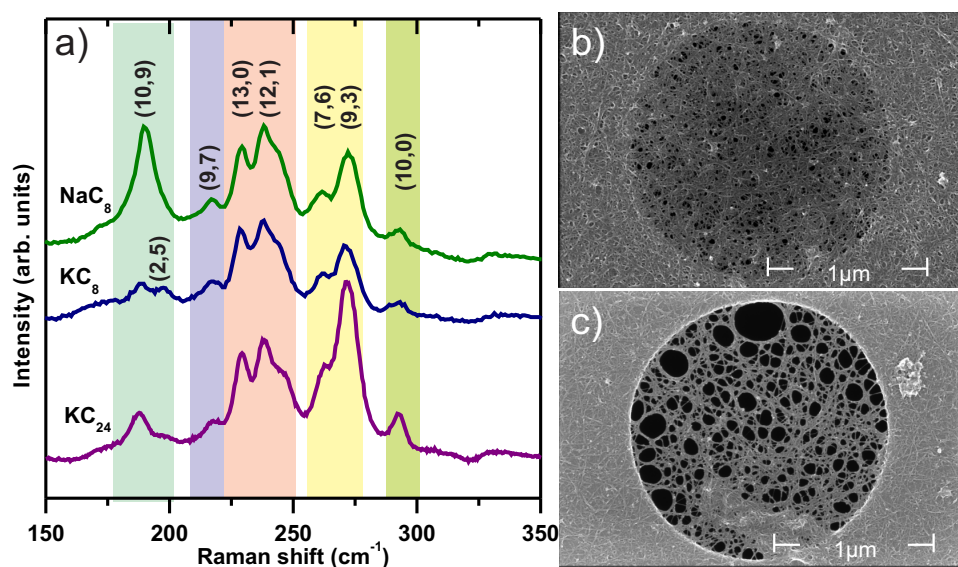


Figure 4.9: GICs from Experiment 2. a) Raman spectra taken with a 532 nm excitation laser of the RBM region, b) SEM image of KC₂₄, c) SEM image of NaC₈.

RBM ω (cm ⁻¹)	RBM ω reference ⁹² (cm ⁻¹)	Diameter (Å)	n	m
186.98	185	12.9	10	9
198.29	199	11.85	12	5
218.62	215	10.88	9	7
229.95	229	10.18	13	0
238.94	237	9.82	12	1
261.33	261	8.83	7	6
272.57	272	8.47	9	3
292.36	292	7.85	10	0

Table 4.3: Experimental RBM frequency and reference RBM frequency (ω) with the corresponding assignment of diameter and (n,m) indices from Experiment 2.

Experiment 2 shows more chiralities according to the Raman spectra (there are more peaks present) in Figure 4.9 a) in comparison with the spectra from Experiment 1 (Figure 4.8 a)). The corresponding SEM images also support this statement. The SEM images presented in Figure 4.8 b) and c) when comparing with Figure 4.9 b) and c) one can notice the effect of the dispersion due to the sonication. While in Experiment 1 a bole of nanotubes is present (with some nanotube ropes coming out that bole), in Experiment 2 meshes have been formed for both KC₂₄ and NaC₈.

The KC₂₄ and NaC₈ from Experiment 2 were placed in a TEM gold grid for the SEM measurement. Figure 4.9 b) corresponds to the SEM image of KC₂₄, here the mesh is more homogeneously dispersed that in NaC₈ (Figure 4.9 c).The sonication process does help to the dispersion and it is better for high stage GIC.

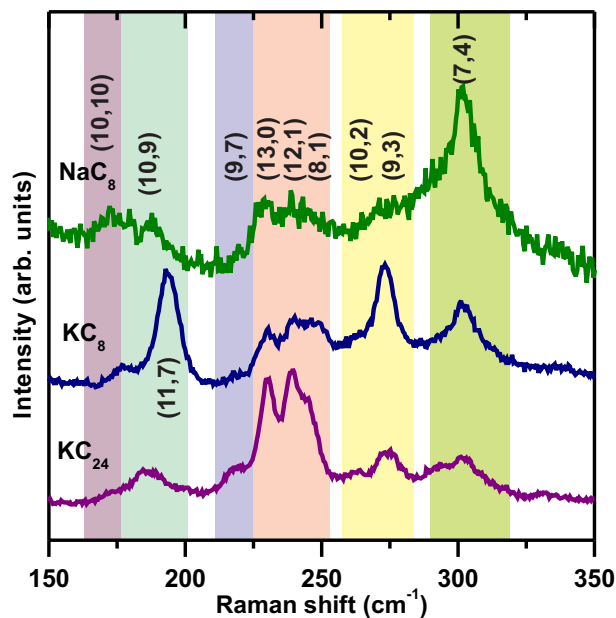


Figure 4.10: Raman spectra taken with a 532 nm excitation laser of the RBM region of GICs from Experiment 3.

RBM ω (cm ⁻¹)	RBM ω reference ⁹² (cm ⁻¹)	Diameter (Å)	n	m
172.84	176	13.57	10	10
186.78	185	12.9	10	0
193.71	192	12.31	11	7
217.54	215	10.88	9	7
229.68	229	10.18	13	0
239.39	237	9.82	12	1
245.41	243	9.53	8	6
263.13	264	8.72	10	2
274.1	272	8.47	9	3
301.53	302	7.55	7	4

Table 4.4: RBM experimental and reference RBM frequency (ω) and the corresponding assignment of diameter and (n,m) indexes for Experiment 3.

From the RBM in the pristine sample (Figure 4.3), only the chiralities (12,1) and (9,3) are present in the Raman spectra related to Experiment 1 (Figure 4.8 a)), chiralities (10,9), (9,7), (12,1), (7,6), (7,6), (9,3) from Experiment 2 (Figure 4.9 a)), and chiralities (10,9), (12,1) and (9,3) from Experiment 3 (Figure 4.10). All of these nanotubes are present for all the intercalation compounds. The fact that some chiralities from the pristine sample are no longer present can be attributed to the dispersion of the intercalation compounds in the solvent. The dispersion of the nanotubes can give rise to Raman signal from other nanotubes that could not be noticed when they were within the bundles (that contain different types of nanotubes).

All the corresponding chiralities are assigned in Tables 4.1, 4.2, 4.3 and 4.4. The corresponding diameters are also assigned. In general, HiPco[®] SWCNTs have a diameter in the range of 8-12 nm, and the nanotubes assigned are in this range.

More nanotubes with different chiralities are present in experiment 3. Although the samples were kept at rest and still the Raman give a sign of dispersion but for NaC₈, the RBMs in the range 150 to 275 cm⁻¹ are not well pronounced. Perhaps the intercalation with K was more efficient than with Na even though they belong to the same family in the periodic table (therefore they have similar properties). They do differ in the size of the ionic radii. Na⁺ has 0.102 nm of ionic radii while K⁺ has 0.138 nm. This might suggest that because the radii of K is bigger, the separation between nanotubes increases.

Chapter 5

Conclusions & Outlook

Begin at the beginning, "the King said, very gravely" and go on till you come to the end: then stop.

Lewis Carroll

The goal of this research project was the individualization of SWCNTs from the pristine powder sample. However, after the characterization techniques of the samples with SEM, AFM and Raman spectroscopy, the corresponding analysis did not show the individualization. However, a different and interesting result was obtained: the formation of meshes in Experiment 2.

When the solvent was just added to the GICs (Experiment 1), the optical image of the samples reveal already a good dispersion and the SEM image still showed a ball of tangled nanotubes with some filaments coming out of the ball.

In Experiment 2, the sonication process allowed a better dispersion of the SWCNTs in the solvent, leading to the formation of an uniform mesh for KC_{24} and meshes with larger gaps and not that homogenous for NaC_8 as the SEM images indicates.

The Raman spectrum of the RBM region from Experiment 3 shows no well defined peaks, probably the five more minutes of sonication caused a structural modification in the system.

Nanotubes with different chiralities were present in the three experiments. The assignment of the RBMs frequencies was done with the tables presented in reference⁹². However, a proper assignment should be done with Resonance Raman Spectroscopy and the corresponding Kataura plot (which indicates the type of nanotube in resonance with the incident laser energy). The

dispersion of the intercalation compounds also contribute the appearance of nanotubes that were not detected in the pristine sample. As the nanotubes are now "spread" in the solvent (and not as powder), the chance of getting a Raman signal from different nanotubes is possible. The samples with no dispersion (Experiment 1) presented only four chiralities, Experiment 2 presented eight and Experiment 3 showed ten chiralities. It is also important to point out that the majority of the nanotubes assigned according to the RBM frequency are semiconducting. But, the lineshape of the G^- of Experiment 1 suggests a metallic behaviour because of the intercalation with the alkali metals.

Although there exist many attempts to achieve the individualization of SWCNT^{96,97}, the one that is proposed in this research project is different for the following reasons:

1. The elaboration of the intercalation compounds of first (NaC_8 and KC_8) and second stage (KC_{24}). With this, Coulombic repulsion of the negatively charged nanotubes made the dispersion possible.
2. The dispersion of SWCNTs in a ultra dried DMF. This polar and organic solvent has good affinity for the nanotubes when intercalated with the alkali metals.
3. Only five minutes at five revolutions per minute of tip sonication already allows a better dispersion and lead to the formation of meshes.

The path that led to Experiment 2 could be the key to the formation of those surprising meshes. Intercalation compounds in SWCNTs can be the next step for tunable properties of SWCNTs. That, in combination with the meshes can indicate a route to the engineering of devices e.g. sensors.

Bibliography

- [1] Lower, S. Chem1 virtual textbook. 1999.
- [2] McNaught, A. D.; McNaught, A. D. *Compendium of chemical terminology*; Blackwell Science Oxford, 1997; Vol. 1669.
- [3] Karfunkel, H. R.; Dressler, T. New hypothetical carbon allotropes of remarkable stability estimated by MNDO solid-state SCF computations. *Journal of the American Chemical Society* **1992**, *114*, 2285–2288.
- [4] Project, W. D. Carbon Nanotubes. 2011; <http://demonstrations.wolfram.com/CarbonNanotubes/>.
- [5] Wilder, J. W.; Venema, L. C.; Rinzler, A. G.; Smalley, R. E.; Dekker, C. Electronic structure of atomically resolved carbon nanotubes. *Nature* **1998**, *391*, 59.
- [6] Iijima, S.; Ichihashi, T. Single-shell carbon nanotubes of 1-nm diameter. *nature* **1993**, *363*, 603.
- [7] Komatsu, N.; Wang, F. A comprehensive review on separation methods and techniques for single-walled carbon nanotubes. *Materials* **2010**, *3*, 3818–3844.
- [8] Harrison, W. A. *Electronic structure and the properties of solids: the physics of the chemical bond*; Courier Corporation, 2012.
- [9] Eatemadi, A.; Daraee, H.; Karimkhanloo, H.; Kouhi, M.; Zarghami, N.; Akbarzadeh, A.; Abasi, M.; Hanifehpour, Y.; Joo, S. W. Carbon nanotubes: properties, synthesis, purification, and medical applications. *Nanoscale Research Letters* **2014**, *9*, 393.

- [10] Fathi, D. A review of electronic band structure of graphene and carbon nanotubes using tight binding. *Journal of Nanotechnology* **2011**, 2011.
- [11] Odom, T. W.; Huang, J.-L.; Kim, P.; Lieber, C. M. Atomic structure and electronic properties of single-walled carbon nanotubes. *Nature* **1998**, 391, 62.
- [12] Zhou, W.; Bai, X.; Wang, E.; Xie, S. Synthesis, structure, and properties of single-walled carbon nanotubes. *Advanced Materials* **2009**, 21, 4565–4583.
- [13] Roche, S. Carbon nanotubes: exceptional mechanical and electronic properties. 2000.
- [14] Dowling, N. E. *Mechanical behavior of materials: engineering methods for deformation, fracture, and fatigue*; Pearson, 2012.
- [15] S. Dresselhaus, M.; Dresselhaus, G.; Avouris, P. *Carbon Nanotubes*; 2001; pp 287–327.
- [16] Dietzel, D.; Faucher, M.; Iaia, A.; Aime, J.; Marsaudon, S.; Bonnot, A.; Bouchiat, V.; Couturier, G. Analysis of mechanical properties of single wall carbon nanotubes fixed at a tip apex by atomic force microscopy. *Nanotechnology* **2005**, 16, S73.
- [17] of Encyclopaedia Britannica, E. Young's modulus. 2019; <https://www.britannica.com/science/Youngs-modulus>.
- [18] Yao, N.; Lordi, V. Young's modulus of single-walled carbon nanotubes. *Journal of Applied Physics* **1998**, 84, 1939–1943.
- [19] Yakobson, B. I.; Brabec, C.; Bernholc, J. Nanomechanics of carbon tubes: instabilities beyond linear response. *Physical Review Letters* **1996**, 76, 2511.
- [20] Xin, Z.; Jianjun, Z.; Zhong-Can, O.-Y. Strain energy and Young's modulus of single-wall carbon nanotubes calculated from electronic energy-band theory. *Physical Review B* **2000**, 62, 13692.
- [21] Properties, E. Young Modulus for some Materials. *The Engineering ToolBox* **2013**,
- [22] Kittel, C.; McEuen, P.; McEuen, P. *Introduction to solid state physics*; Wiley New York, 1976; Vol. 8.

- [23] Ullrich, C. A. *Time-dependent density-functional theory: concepts and applications*; OUP Oxford, 2011.
- [24] Proctor, J. E.; Armada, D. M.; Vijayaraghavan, A. *An introduction to graphene and carbon nanotubes*; CRC Press, 2017.
- [25] Cardona, M. Optical properties and electronic density of states. *J. Res. Nat. Bur. Stand* **1970**, 253–265.
- [26] Javey, A.; Kong, J. *Carbon nanotube electronics*; Springer Science & Business Media, 2009.
- [27] Chen, G. Optical properties of carbon nanotubes. Ph.D. thesis, The Pennsylvania State University, 2003.
- [28] Charlier, J.-C.; Blase, X.; Roche, S. Electronic and transport properties of nanotubes. *Reviews of Modern Physics* **2007**, 79, 677.
- [29] Kuzmany, H.; Plank, W.; Hulman, M.; Kramberger, C.; Grüneis, A.; Pichler, T.; Peterlik, H.; Kataura, H.; Achiba, Y. Determination of SWCNT diameters from the Raman response of the radial breathing mode. *The European Physical Journal B-Condensed Matter and Complex Systems* **2001**, 22, 307–320.
- [30] Kataura, H.; Kumazawa, Y.; Maniwa, Y.; Umezumi, I.; Suzuki, S.; Ohtsuka, Y.; Achiba, Y. Optical properties of single-wall carbon nanotubes. *Synthetic metals* **1999**, 103, 2555–2558.
- [31] Kong, J.; Cassell, A. M.; Dai, H. Chemical vapor deposition of methane for single-walled carbon nanotubes. *Chemical Physics Letters* **1998**, 292, 567–574.
- [32] Arora, N.; Sharma, N. Arc discharge synthesis of carbon nanotubes: Comprehensive review. *Diamond and Related Materials* **2014**, 50, 135–150.
- [33] Arepalli, S. Laser ablation process for single-walled carbon nanotube production. *Journal of nanoscience and nanotechnology* **2004**, 4, 317–325.

- [34] Chrzanowska, J.; Hoffman, J.; Małolepszy, A.; Mazurkiewicz, M.; Kowalewski, T. A.; Szymanski, Z.; Stobinski, L. Synthesis of carbon nanotubes by the laser ablation method: Effect of laser wavelength. *physica status solidi (b)* **2015**, *252*, 1860–1867.
- [35] Nikolaev, P.; Bronikowski, M. J.; Bradley, R. K.; Rohmund, F.; Colbert, D. T.; Smith, K.; Smalley, R. E. Gas-phase catalytic growth of single-walled carbon nanotubes from carbon monoxide. *Chemical Physics Letters* **1999**, *313*, 91–97.
- [36] Kong, J.; Soh, H. T.; Cassell, A. M.; Quate, C. F.; Dai, H. Synthesis of individual single-walled carbon nanotubes on patterned silicon wafers. *Nature* **1998**, *395*, 878.
- [37] Nanointegers, I. Nanointegers. 2019; <http://nanointegris.com>.
- [38] Choudhary, V.; Singh, B.; Mathur, R. *Syntheses and applications of carbon nanotubes and their composites*; IntechOpen, 2013.
- [39] Girifalco, L.; Hodak, M.; Lee, R. S. Carbon nanotubes, buckyballs, ropes, and a universal graphitic potential. *Physical Review B* **2000**, *62*, 13104.
- [40] gmbh, H. U. How To Disperse Single-Walled Carbon Nanotubes Individually. 1999; <https://www.hielscher.com/how-to-disperse-single-walled-carbon-nanotubes-individually.htm>.
- [41] Vaisman, L.; Wagner, H. D.; Marom, G. The role of surfactants in dispersion of carbon nanotubes. *Advances in Colloid and Interface Science* **2006**, *128*, 37–46.
- [42] Grossiord, N.; van der Schoot, P.; Meuldijk, J.; Koning, C. E. Determination of the surface coverage of exfoliated carbon nanotubes by surfactant molecules in aqueous solution. *Langmuir* **2007**, *23*, 3646–3653.
- [43] Tan, Y.; Resasco, D. E. Dispersion of single-walled carbon nanotubes of narrow diameter distribution. *The Journal of Physical Chemistry B* **2005**, *109*, 14454–14460.
- [44] Wang, H. Dispersing carbon nanotubes using surfactants. *Current Opinion in Colloid & Interface Science* **2009**, *14*, 364–371.

- [45] Pramanik, C.; Gissinger, J. R.; Kumar, S.; Heinz, H. Carbon nanotube dispersion in solvents and polymer solutions: mechanisms, assembly, and preferences. *ACS nano* **2017**, *11*, 12805–12816.
- [46] Nguyen, T. T.; Nguyen, S. U.; Phuong, D. T.; Nguyen, D. C.; Mai, A. T. Dispersion of denatured carbon nanotubes by using a dimethylformamide solution. *Advances in Natural Sciences: Nanoscience and Nanotechnology* **2011**, *2*, 035015.
- [47] Naidu, M. *Engineering Physics*; Pearson Education India, 2009.
- [48] Rossi, J. E.; Soule, K. J.; Cleveland, E.; Schmucker, S. W.; Cress, C. D.; Cox, N. D.; Merrill, A.; Landi, B. J. Removal of sodium dodecyl sulfate surfactant from aqueous dispersions of single-wall carbon nanotubes. *Journal of Colloid and Interface Science* **2017**, *495*, 140–148.
- [49] Boehm, H. P.; Setton, R.; Stumpp, E. Nomenclature and terminology of graphite intercalation compounds (IUPAC Recommendations 1994). *Pure and Applied Chemistry* **1994**, *66*, 1893–1901.
- [50] Dresselhaus, M.; Dresselhaus, G. Intercalation compounds of graphite. *Advances in Physics* **1981**, *30*, 139–326.
- [51] Fischer, J. E.; Thompson, T. E. Graphite intercalation compounds. *Physics Today* **1978**, *31*, 36–45.
- [52] D.D.L.Chung, *Encyclopedia of Materials: Science and Technology*; Elsevier, 2001.
- [53] Chung, D. Graphite intercalation compounds. *Encyclopedia of Materials: Science and Technology* **2016**, 3641–3645.
- [54] Vecera, P.; Chacón-Torres, J. C.; Pichler, T.; Reich, S.; Soni, H. R.; Görling, A.; Edelhahammer, K.; Peterlik, H.; Hauke, F.; Hirsch, A. Precise determination of graphene functionalization by in situ Raman spectroscopy. *Nature communications* **2017**, *8*, 15192.
- [55] Neha, B.; Manjula, K.; Srinivasulu, B.; Subhas, S. C. Synthesis and characterization of exfoliated graphite/ABS composites. *Open Journal of Organic Polymer Materials* **2012**, *2*, 75.

- [56] Aqel, A.; El-Nour, K. M. A.; Ammar, R. A.; Al-Warthan, A. Carbon nanotubes, science and technology part (I) structure, synthesis and characterisation. *Arabian Journal of Chemistry* **2012**, *5*, 1–23.
- [57] Tasis, D. *Carbon nanotube-polymer composites*; Royal Society of Chemistry, 2013; Vol. 27.
- [58] Duclaux, L.; Salvétat, J.; Lauginie, P.; Cacciaguera, T.; Faugere, A.; Goze-Bac, C.; Bernier, P. Synthesis and characterization of SWNT-heavy alkali metal intercalation compounds, effect of host SWNTs materials. *Journal of Physics and Chemistry of Solids* **2003**, *64*, 571–581.
- [59] Pichler, T.; Sing, M.; Knupfer, M.; Golden, M.; Fink, J. Potassium intercalated bundles of single-wall carbon nanotubes: electronic structure and optical properties. *Solid state communications* **1999**, *109*, 721–726.
- [60] Bower, C.; Suzuki, S.; Tanigaki, K.; Zhou, O. Synthesis and structure of pristine and alkali-metal-intercalated single-walled carbon nanotubes. *Applied Physics A* **1998**, *67*, 47–52.
- [61] Rao, A. M.; Eklund, P.; Bandow, S.; Thess, A.; Smalley, R. E. Evidence for charge transfer in doped carbon nanotube bundles from Raman scattering. *Nature* **1997**, *388*, 257.
- [62] Liu, G.; Zhao, Y.; Zheng, K.; Liu, Z.; Ma, W.; Ren, Y.; Xie, S.; Sun, L. Coulomb explosion: a novel approach to separate single-walled carbon nanotubes from their bundle. *Nano Letters* **2008**, *9*, 239–244.
- [63] others., *et al. Scanning electron microscopy, X-ray microanalysis, and analytical electron microscopy: a laboratory workbook*; Springer Science & Business Media, 2012.
- [64] Kulkarni, V. S.; Shaw, C. *Essential Chemistry for Formulators of Semisolid and Liquid Dosages*; Academic Press, 2015.
- [65] Loos, J. The art of SPM: Scanning probe microscopy in materials science. *Advanced Materials* **2005**, *17*, 1821–1833.
- [66] Martin, Y.; Wickramasinghe, H. K. Magnetic imaging by "force microscopy" with 1000 Å resolution. *Applied Physics Letters* **1987**, *50*, 1455–1457.

- [67] Rugar, D.; Hansma, P. Atomic force microscopy. *Physics Today* **1990**, *43*, 23–30.
- [68] Meyer, G.; Amer, N. M. Novel optical approach to atomic force microscopy. *Applied Physics Letters* **1988**, *53*, 1045–1047.
- [69] van der Meer, F. Near-infrared laboratory spectroscopy of mineral chemistry: A review. *International journal of applied earth observation and geoinformation* **2018**, *65*, 71–78.
- [70] Hulman, M. *Graphene*; Elsevier, 2014; pp 156–183.
- [71] Born, M.; Huang, K. *Dynamical theory of crystal lattices*; Clarendon press, 1954; p 367.
- [72] Raman, C. V.; Krishnan, K. S. A new type of secondary radiation. *Nature* **1928**, *121*, 501.
- [73] Staveley, L. A. K. *The characterization of chemical purity: organic compounds*; Elsevier, 2016.
- [74] Merlin, R.; Pinczuk, A.; Weber, W. *Raman scattering in materials science*; Springer, 2000; pp 1–29.
- [75] Hulman, M. *Graphene: properties, preparation, characterisation and devices*; 2014.
- [76] Best, S. P.; Clark, R. J.; Withnall, R. Non-destructive pigment analysis of artefacts by Raman microscopy. *Endeavour* **1992**, *16*, 66–73.
- [77] Rodriguez-Nieva, J.; Barros, E.; Saito, R.; Dresselhaus, M. Disorder-induced double resonant Raman process in graphene. *Physical Review B* **2014**, *90*, 235410.
- [78] Lazzeri, M.; Piscanec, S.; Mauri, F.; Ferrari, A.; Robertson, J. Phonon linewidths and electron-phonon coupling in graphite and nanotubes. *Physical Review B* **2006**, *73*, 155426.
- [79] Beams, R.; Cançado, L. G.; Novotny, L. Raman characterization of defects and dopants in graphene. *Journal of Physics: Condensed Matter* **2015**, *27*, 083002.
- [80] others,, *et al.* G-band resonant Raman study of 62 isolated single-wall carbon nanotubes. *Physical Review B* **2002**, *65*, 155412.

- [81] Dresselhaus, M. S.; Dresselhaus, G.; Saito, R.; Jorio, A. Raman spectroscopy of carbon nanotubes. *Physics reports* **2005**, *409*, 47–99.
- [82] others., *et al.* Diameter-selective Raman scattering from vibrational modes in carbon nanotubes. *Science* **1997**, *275*, 187–191.
- [83] Sattler, K. D. *Handbook of nanophysics: nanotubes and nanowires*; CRC Press, 2010.
- [84] Kürti, J.; Zólyomi, V.; Grüneis, A.; Kuzmany, H. Double resonant Raman phenomena enhanced by van Hove singularities in single-wall carbon nanotubes. *Physical Review B* **2002**, *65*, 165433.
- [85] Tyborski, C.; Vierck, A.; Narula, R.; Popov, V. N.; Maultzsch, J. Double-resonant Raman scattering with optical and acoustic phonons in carbon nanotubes. *Physical Review B* **2018**, *97*, 214306.
- [86] Pimenta, M.; Dresselhaus, G.; Dresselhaus, M. S.; Cancado, L.; Jorio, A.; Saito, R. Studying disorder in graphite-based systems by Raman spectroscopy. *Physical chemistry chemical physics* **2007**, *9*, 1276–1290.
- [87] Thomsen, C.; Reich, S. Double resonant Raman scattering in graphite. *Physical Review Letters* **2000**, *85*, 5214.
- [88] others., *et al.* Linewidth of the Raman features of individual single-wall carbon nanotubes. *Physical Review B* **2002**, *66*, 115411.
- [89] Jorio, A.; Pimenta, M.; Souza Filho, A.; Saito, R.; Dresselhaus, G.; Dresselhaus, M. Characterizing carbon nanotube samples with resonance Raman scattering. *New Journal of Physics* **2003**, *5*, 139.
- [90] Dresselhaus, M. S.; Dresselhaus, G. Intercalation compounds of graphite. *Advances in Physics* **2002**, *51*, 1–186.
- [91] Rosario-Castro, B. I.; Contés, E. J.; Lebrón-Colón, M.; Meador, M. A.; Sánchez-Pomales, G.; Cabrera, C. R. Combined electron microscopy and spectroscopy characterization of as-received, acid purified, and oxidized HiPCO single-wall carbon nanotubes. *Materials Characterization* **2009**, *60*, 1442–1453.

- [92] Maultzsch, J.; Telg, H.; Reich, S.; Thomsen, C. Radial breathing mode of single-walled carbon nanotubes: Optical transition energies and chiral-index assignment. *Physical Review B* **2005**, *72*, 205438.
- [93] Ferrari, A. C.; Robertson, J. Interpretation of Raman spectra of disordered and amorphous carbon. *Physical Review B* **2000**, *61*, 14095.
- [94] Kastner, J.; Pichler, T.; Kuzmany, H.; Curran, S.; Blau, W.; Weldon, D.; Delamesiere, M.; Draper, S.; Zandbergen, H. Resonance Raman and infrared spectroscopy of carbon nanotubes. *Chemical Physics Letters* **1994**, *221*, 53–58.
- [95] Chacon-Torres, J. C.; Wirtz, L.; Pichler, T. Manifestation of charged and strained graphene layers in the Raman response of graphite intercalation compounds. *ACS Nano* **2013**, *7*, 9249–9259.
- [96] Liu, H.; Nishide, D.; Tanaka, T.; Kataura, H. Large-scale single-chirality separation of single-wall carbon nanotubes by simple gel chromatography. *Nature communications* **2011**, *2*, 309.
- [97] Tanaka, T.; Jin, H.; Miyata, Y.; Kataura, H. High-yield separation of metallic and semi-conducting single-wall carbon nanotubes by agarose gel electrophoresis. *Applied physics express* **2008**, *1*, 114001.